NTNU
Norwegian University
of Science and Technology

Department of Energy
and Process Engineering

EPT-M-2013-15

MASTER THESIS

for

Stud.techn. Nikolai Austarheim

Spring 2013

DNS of acoustic instabilities in low emission combustion systems

DNS av akustiske instabiliteter fra forbrenning i lavutslipps energisystemer

Background and objective

Recently much research has been devoted to using natural gas or other hydrogen rich gaseous fuels in new state-of-the-art gas turbines for power production. The fuels are associated with low CO2 emissions, and their use characterized by a high efficiency when combustion takes place in advanced combustion chambers operating in Lean Pre-Mixed (LPM) mode. One of the major challenges related to combustion in the LPM-regime is however efficient and reliable control of the acoustic instabilities, combustion noise, associated with LPM combustion. Such combustion noise can in severe cases have a disruptive effect on the burner. Locally colliding flame fronts are believed to be one of the main sources for acoustic waves; however much is still unknown about how pressure and fuel composition affect this phenomenon. The modest understanding we have of the origin and behaviour of combustion noise today is a limiting factor when carrying out reliable turbine combustion modelling.

Direct numerical simulations will be used to study colliding flame fronts. A pre-study has been made using a 1D configuration; however issues related to preferential diffusion and 2D/3D effects are to be addressed.

The work is related to the activities within the international research centre BIGCCS, and is in close collaboration with Sintef Energy AS and with Sandia National Laboratories, US. A study trip to Sandia Nat. Labs. is planned during the course of this work. The work is a continuation of the candidate's project thesis.

The following tasks are to be considered:

1. Modification and validation of DNS code for 2D imploding flame fronts. This involves adapation of consistantly similar boundary conditions.
2. Identification of modelling conditions for 2D simulations.
3. Carry out simulations on HPC facilities for 2D imploding flame fronts.
4. Possible 3D cases will be studied if time allows.
5. Analysis of results and identification of driving parameters for instabilities.

-- " --

Within 14 days of receiving the written text on the master thesis, the candidate shall submit a research plan for his project to the department.

When the thesis is evaluated, emphasis is put on processing of the results, and that they are presented in tabular and/or graphic form in a clear manner, and that they are analyzed carefully.

The thesis should be formulated as a research report with summary both in English and Norwegian, conclusion, literature references, table of contents etc. During the preparation of the text, the candidate should make an effort to produce a well-structured and easily readable report. In order to ease the evaluation of the thesis, it is important that the cross-references are correct. In the making of the report, strong emphasis should be placed on both a thorough discussion of the results and an orderly presentation.

The candidate is requested to initiate and keep close contact with his/her academic supervisor(s) throughout the working period. The candidate must follow the rules and regulations of NTNU as well as passive directions given by the Department of Energy and Process Engineering.

Risk assessment of the candidate's work shall be carried out according to the department's procedures. The risk assessment must be documented and included as part of the final report. Events related to the candidate's work adversely affecting the health, safety or security, must be documented and included as part of the final report. If the documentation on risk assessment represents a large number of pages, the full version is to be submitted electronically to the supervisor and an excerpt is included in the report.

Pursuant to "Regulations concerning the supplementary provisions to the technology study program/Master of Science" at NTNU §20, the Department reserves the permission to utilize all the results and data for teaching and research purposes as well as in future publications.

The final report is to be submitted digitally in DAIM. An executive summary of the thesis including title, student's name, supervisor's name, year, department name, and NTNU's logo and name, shall be submitted to the department as a separate pdf file. Based on an agreement with the supervisor, the final report and other material and documents may be given to the supervisor in digital format.

☐ Work to be done in lab (Water power lab, Fluids engineering lab, Thermal engineering lab)
☐ Field work

Department of Energy and Process Engineering, 14. January 2013

Olav Bolland
Department Head

Terese Løvås
Academic Supervisor

Research Advisors: Dr. Nils E. Haugen (Sintef Energy), Andrea Gruber (Sintef Energy).

Preface

This master thesis builds further on the summer assignment (at SINTEF Energy, Trondheim, 2012) and project work in the fall of 2012 of Nikolai Austarheim. In the summer assignment the physics and order of the pressure drop at impact for two opposing hydrogen-air flames in one dimension was investigated using Direct Numerical Simulations (DNS). In the project the work with opposing flames were continued and expanded. It was originally ment to cover two dimensional simulations, but due to boundary problems this was postponed to the master thesis. The work therefore consisted mainly of comparison between simple and detailed chemistry representation.

This master thesis, *DNS of acoustic instabilities in low emission combustion systems*, was produced at the Department of Energy and Process Engineering at the Norwegian University of Science and Technology (NTNU) in Trondheim, Norway, in cooperation with SINTEF Energy, Trondheim.

The objective of this master thesis was to investigate the sound generation of flame annihilation in a two dimensional setting using premixed hydrogen-air as fuel. This is done to enhance the knowledge of sound generation in combustion chambers in modern gas turbines. A detailed chemistry representation has been used, and DNS was the tool for investigating the hydrogen-air flames under given conditions.

Although the work has not always been simple, straightforward, or gone according to plan, it has been a very interesting experience working on this thesis. I have, as most master students, been frustrated at times, but giving up has never been an option.

I would like to thank my supervisors, Terese Løvås at NTNU, and Andrea Gruber and Nils E. Haugen at SINTEF, for their invaluable experience and considerate nature. Their knowledge, guidance and help has been a great inspiration. I would also like to show my gratitude to SINTEF Energy for letting me use their computer cluster. Also, a special thanks goes to Hemanth Kolla at Sandia National Laboratories for providing the necessary source file for performing the simulations and Troels A. Bojesen at NTNU for proofreading the thesis and thus providing some much appreciated help.

Nikolai Austarheim
Trondheim, 10th June, 2013

Abstract

In a state of the art gas turbine using Lean Pre-Mixed fuels one of the main challenges is efficient and reliable control of sound generated during combustion. Knowledge of sound generation in gas turbine combustion chambers has to be enhanced in order to develop a reliable model with predictive capabilites.

In this thesis Direct Numerical Simulations (DNS) of two dimensional laminar imploding circular flame fronts have been performed. One dimensional simulations of laminar opposing flame fronts have been performed to establish modeling conditions for the two dimensional simulations, evaluate the boundary influence on the simulations and provide comparable simulation results. In addition a pre-study for three dimensional simulation of an inwards burning sphere of fuel has been done. The motivation of this thesis is to enhance the knowledge related to generation of acoustic waves in the combustion chamber of a gas turbine.

The S3D code (a parallel DNS code for solving reactive flows) was modified to include two dimensional circular imploding flame fronts. A thorough investigation to validate the boundary influence on the annihilation event is recommended. This is due to simulations which indicate that the boundary conditions may influence especially the pressure drop after time of impact.

In two dimensions DNS have been performed at pressure 1 atm for fuel equivalence ratios 0.3, 0.5, 0.8 and 1.5 with detailed chemistry representation. Care has been taken to ensure adequat resolution of the flame (a minimum of ten points over the flame). The results from the simulations were used to measure key parameters (as the pressure drop after impact, the laminar flame speed, etc.). The following trends were found for the two dimensional simulations with increasing fuel equivalence ratio (ϕ) (in the given range of ϕ's): The flame thickness, unburned and burned gas density decrease, while the fluid expansion velocity, laminar flame speed, propagation speed of the pressure wave, pressure difference before the flame fronts meet, pressure drop after impact and burned temperature increase. This coincides with the the trends in the one dimensional simulations, and is consistent with the given theory.

The results were compared with analytical relations developed in the candidate's project work of fall 2012. It was found that the three relations gave a poor impression of the measured values.

It is indicated that to fully understand the annihilation process a number of simulations have to be run. The propagation speed of the pressure wave, the fluid expansion velocity and the pressure drop after time of impact require special attention.

Sammendrag

I en moderne gassturbin som bruker Lean Pre-Mixed brennstoff er en av hovedutfordringene effektiv og pålitelig kontroll av lyd generert i forbindelse med forbrenningen. Kunnskap om lydgenereringen i brennkammeret i gassturbiner må forbedres slik at man kan utvikle en pålitelig modell med predikative egenskaper.

I denne masteroppgaven er Direkte Numeriske Simuleringer (DNS) av to-dimensjonale, laminære, imploderende, sirkulære flammefronter gjennomført. En-dimensjonale simuleringer av laminære, møtende flammefronter har blitt gjort for å etablere simuleringsforholdene til de to-dimensjonale simuleringene, vurdere domenegrensenes innflytelse på resultatene, og for å være sammenlignbart materiale. I tillegg er en forstudie for tre-dimensjonal simulering av en innover-brennende flamme-sfære gjort. Motivasjonen var å øke kunnskapen rundt lydgenerering i brennkammeret i gassturbiner under forbrenning.

S3D-koden (en parallell DNS-kode for å simulere reaktive strømninger) ble endret for å inkludere to-dimensjonale, sirkulære, imploderende flammefronter. En dyptgående analyse for å vurdere innflytelsen til domenegrensene på selve annihilerings-prosessen er anbefalt. Dette er anbefalt på bakgrunn av simuleringer som indikerer at domengrensene påvirker spesielt trykkfallet etter at flammene har møttes.

DNS i to dimensjoner med detaljert kjemisk representasjon har blitt gjort ved trykk 1 atm og ved ekvivalens-forhold 0.3, 0.5, 0.8 og 1.5. Oppløsningen til flammene har blitt sikret ved å kreve minst ti punkter over flammen. Simuleringene ble brukt til å måle nøkkelparametre (trykkfall etter møte, laminær flammehastighet, etc.). Følgende trender ble observert for de to-dimensjonale simuleringene ved økende ekvivalens-forhold (ϕ) (for gitte verdier av ϕ): Flammetykkelsen, tettheten i det ubrente og brente området øker, mens fluidets ekspansjonshastighet, den laminære flammehastigheten, propageringshastigheten til trykkbølgen, trykkdifferasnen før flammefrontene møtes, trykkfallet etter flammefrontene møtes og temperaturen i det brente området øker.

Resultatene ble sammenlignet med de analytiske relasjoner utviklet i kandidatens prosjektarbeid høsten 2012. Det ble funnet at de tre relasjonene gav et generelt dårlig inntrykk av de målte verdiene (store avvik).

Det er indikert at for å få en full oversikt og forstå annihilerings-prosessen må flere simuleringer kjøres. Spesielt propageringshastigheten til trykkbølgen, fluidets ekspansjonshastighet, og trykkfallet etter møte krever videre arbeid.

Nomenclature

Latin letters

A	Area	[m^2]
$\bar{A}$	Time smoothed flame area	[m^2]
B_0	Pre-exponential factor	Various units
c_b	Sonic velocity	[m/s]
c_p	Specific heat capacity at constant pressure	[J/kgK]
C_s	Speed of sound	[m/s]
D	Mass diffusivity	[m^2/s]
e_0	Specific total energy	[J/kg]
e_t	Specific total internal energy	[J/kg]
E_a	Activation energy	[J/mol]
$\vec{f}_i$	Body forces on species i, vector notation	[m/s^2]
$\vec{g}$	Gravitational acceleration, vector notation	[m/s^2]
I	Identity matrix	-
k	Thermal conductivity	[W/mK]
k_G	Global reaction rate coefficient	Various units
L	Length	[m]
L_x, L_y, L_z	Length of the domain in x-, y-, z-direction	[m]
Le	Lewis number	-
m_{ox}	Mass of oxidizer in fuel-oxidizer mixture	[kg]
m_{fuel}	Mass of fuel in fuel-oxidizer mixture	[kg]
$\dot{m}$	Mass flow rate	[kg/s]
$\dot{m}''$	Mass flow rate flux	[kg/ms^2]
n	Overall reaction order	-
N_x, N_y, N_z	Number of grid points in x-, y-, z-direction	-
P	Pressure	[atm, Pa]
q	Heat flux	[W/m^2]
Q	Specific heat of reaction	[m^2/s^2]
Re	Reynolds number	-
R_u	Universal gas constant	[J/mol K]
S_L	Laminar flame speed	[m/s]
S_t	Turbulent flame speed	[m/s]
T	Temperature	[K]
T_b	Temperature in the burned domain	[K]
T_u	Temperature in the unburned domain	[K]
t	Time	[s]

t_{step}	Timestep in simulations	[s]
u	Velocity	[m/s]
$\vec{u}$	Velocity, vector notation	[m/s]
u_b	Fluid expansion velocity	[m/s]
u_p	Propagation speed of pressure wave	[m/s]
v_b	Burned gas velocity	[m/s]
v_u	Unburned gas velocity	[m/s]
x_i	Spatial coordinate, tensor notation	[m]
$[X_i]$	Molar concentration of species i	[mol/m^3]
Y	Unburned fuel mass fraction	-
Y_i	Mass fraction of species i	-

Greek symbols

α	Thermal diffusivity	[m^2/s]
δ_a	Pressure wave propagation length scale	[m]
δ_f	Flame thickness	[m]
δ_L	Laminar flame thickness	[m]
ζ	Spatial coordinate	[m]
Θ	Reduced temperature	-
λ	Second viscosity coefficient	[kg/ms]
μ	Dynamic viscosity	[kg/ms]
ν	Kinematic viscosity	[m^2/s]
ρ	Density	[kg/m^3]
ρ_b	Burned gas density	[kg/m^3]
ρ_u	Unburned gas density	[kg/m^3]
τ_a	Pressure wave propagation time scale	[s]
τ_f	Flame propagation time scale	[s]
τ	Shear stress	[Pa]
$\underline{\tau}$	Stress tensor	[Pa]
$\tau_{\zeta\zeta}$, $\tau_{\phi\phi}$	Stress tensors	[Pa]
ϕ	Fuel equivalence ratio	-
$\dot{\omega}$	Chemical reaction rate	[mol/ms]

Contents

List of Figures

List of Tables

1 Introduction

Combustion of fossil fuels is the number one source of energy in the world, with about 90% of the total energy use (Turns [41]). Electricity generation, transport systems and industrial processes are all highly dependent on combustion. With the increasing energy demands of the world [1], gas turbines are ever more used, both in industrial plants and in power generation.

The development of gas turbines from the early postulates in the first decade of the twentieth century, to the first realizations of the gas turbine in the late 1930s, to today, has been a steady and continuous progress. The early gas turbines for power generation had a low thermal efficiency and power output. These drawbacks ment that gas turbines in non-aircraft markets did not make a real impact before the end of the 20th century. Saravanamuttoo et al. [34] and Gupta [16] gives a short overview of gas turbine development.

Despite the massive development in gas turbine combustion, there are still significant emissions related to the combustion process. To reduce the environmental damage due to gas turbine combustion, improvement and optimization of the gas turbine itself is therefore necessary and important. The products of combustion of fossil fuels are recognised as a source of severe environmental damage. The pollutants mainly consists of unburned hydrocarbons, nitrogen oxides, carbon monoxide, sulfur oxides and particulate matter, while the major combustion product of hydrocarbons are carbon dioxide and water. The aim for future gas turbines should be complete combustion (no unburned hydrocarbons), lower NO_x emissions, and higher thermal efficiency.

Saravanamuttoo et al. [34] identifies three main methods for reducing emissions in a gas turbine system:

- Water or steam injection, which will provide a substantial decrease in flame temperature.
- Selective catalytic reduction, which is a system for exhaust clean up where a catalyst is used together with injection of controlled amounts of ammonia resulting in the conversion of NO_x to N_2 and H_2O.
- Dry low NO_x, which utilize combustors capable of operation at low levels of NO_x without any requirement for water.

Also one should have in mind the fuels used and the processing of combustion products. An alternative to natural gas is hydrogen. Hydrogen can be produced from gasification of coal. Gasification of coal is the reaction between coal, oxygen

and steam to produce hydrogen and carbon monoxide. The carbon monoxide is called a syngas, which can react further with water vapour to form hydrogen and carbon dioxide. The hydrogen can then be combusted in a gas turbine with water as the only product, while the carbon dioxide is removed and sequestrated.

When it comes to combustion of hydrogen in gas turbines there are some major challenges:

- High flame speed.
- High flame temperature.
- Difficulties in stabilizing the flame.

Hydrogen is a very light molecule. It has a high molecular and thermal diffusivity and is very reactive with a large flammability range (Ströhle and Myhrvold [36]). To get to grips with these challenges detailed knowledge of hydrogen combustion is needed.

The state of the art gas turbines are characterized by high thermal efficiencies and advanced combustion chambers operating in Lean Pre-Mixed (LPM) mode. One of the main challenges is efficient and reliable control of sound which is generated during LPM combustion. The flame in such a combustion chamber is virtually at the brink of extinction and therefore knowledge of combustion noise is very important. Combustion noise is of today the largest obstacle in being able to develop a reliable model with predictive capabilities of sound generation in the gas turbine combustion chamber. This is due to the instability the sound generated introduce in the system. This will influence the system both upstream and downstream as the propagation of sound is faster than the propagation of fuel.

Knowledge of sound generation in gas turbine combustion chambers has to be enhanced in order to develop these models. Research has to be done for a large variety of fuels and gas turbine systems. This is no easy task as the flow is usually turbulent and the chemistry is complex in a gas turbine combustion chamber.

One tool to obtain the needed knowledge is numerical simulations. Significant improvements in computer hardware and computational algorithms makes it possible to numerically study increasingly complex cases. One such method is Direct Numerical Simulations (DNS). Unlike Reynolds Averaged Navier-Stokes (RANS), DNS does not use any turbulence models. RANS will solve a mean quantity of the flow, while DNS solves the governing equations for a time-dependent velocity field for one realization of the turbulent flow. DNS is the

most advanced and accurate numerical tool for turbulent combustion, but it is also computationally expensive and restricted to simple flows. In Moin and Mahesh [27] DNS of turbulent flows is thoroughly reviewed.

DNS is a method to simulate reactive flows in great detail and is optimal to study formation and interactions of pressure waves (sound) by a laminar or turbulent flame front. Especially important in this context is to understand the transient processes that occur when two flame fronts collide and merge.

The complexity of the chemistry also adds to the computational expensiveness. The chemical reactions has to be resolved in addition to the fluids motion. In a combustion process with hydrogen and air as the reactants, the products will be heat and water. The complete reaction mechanism however consists of 19 reactions (see section 2.3). There are several ways to deal with the added layer of complexity with chemical reactions, from single-step models to detailed chemistry taking a given number of species and elementary reactions into account.

This report will focus on DNS of colliding flame fronts with the motivation of studying generation of acoustic waves related to this process (which occur for instance in the combustion chamber of a stationary gas turbine). The study will be constricted to premixed hydrogen combustion under laminar conditions. DNS is chosen due to comparison with later works and because it is the most accurate tool for these kind of simulations. The main focus will be on two dimensional simulations, but one dimensional and three dimensional simulations will also be utilized and attempted, respectively.

This master thesis is a continuation of the candidate's project work in the fall of 2012.

The thesis consists of five main parts:

- Modification and validation of DNS code for two dimensional imploding flame fronts. This involves adaptation of consistantly similar boundary conditions.
- Identification of modeling conditions for two dimensional simulations.
- Carry out simulations on for two dimensional imploding flame fronts.
- A pre-study for three dimensional simulations.
- Analysis of results and identification of driving parameters for instabilities.

This thesis will have the following structure: First the general theory of flow, combustion (and combustion chemistry), hydrogen fundamentals, thermoacoustic oscillations and the governing equations will be covered. The theory chapter is

followed by relevant prior work, which will work as a foundation in the analytical study and as comparative material in the numerical study. In prior work numerical and analytical work on reacting flows will be covered. This is followed by an analytical study, where some simple relations are uncovered and relations from other studies are presented. Then the numerical method is presented, followed by the results from the numerical studies. The results is then compared both with works by other authors, the relations uncovered in the analytical study, the results from the one dimensional simulations of the project work (by the candidate in fall 2012), and the theory. The results are discussed, conclusions drawn, and further work is suggested.

2 Theory

In this chapter the underlying theory is presented. Flow, combustion, hydrogen fundamentals, thermoacoustic oscillations and governing equations are covered in the given order to give a thorough base for understanding the problem at hand. These subjects are ment to give a total overview of the basic theory of reactive flows in relation to gas turbines, and give insight into the problems related to hydrogen-fueled gas turbines.

2.1 Flow

In this report flow is the movement of fluids in a domain. Flow in everyday life can be a waterfall, a river, the wind, etc. A fluid is defined by the fact that a fluid cannot resist a shear stress by a static deflection. There are two types of fluids, liquids and gases. A liquid's molecules are closely spaced while a gas' molecules are widely spaced (White [45]).

In this report the focus is on hydrogen-air gas. Initially the hydrogen-air gas is at rest, but a velocity out of the domain (from the unburned to burned domain) is induced by temperature gradients. In fig. 2.1 the temperature, fluid expansion velocity and density is presented when the flame fronts are not affecting each other (the flame fronts propagate towards the center of the domain), mainly to serve as a visualization of the flame fronts. The simulations in this thesis therefore involves both fluids at rest, in motion, and which is exposed to a combustion process. The problem is also further complicated by the introduction of detailed chemistry.

2.1.1 Flow Characteristics

One of the most known parameters to characterize flow is the Reynolds number, Re. This is defined as:

$$\mathrm{Re} = \frac{uL}{\nu}, \tag{2.1}$$

where u and L are the velocity and length scales of the flow, respectively, and ν is the kinematic viscosity (White [45]). The Reynolds number correlates the viscous behaviour of all newtonian fluids. Viscosity is a quantitative measure of a fluid's resistance to flow, in other words it determines the fluid strain rate that is generated by a given applied shear stress. For a newtonian fluid the shear stress is proportional to the velocity gradient (when u is perpendicular to the

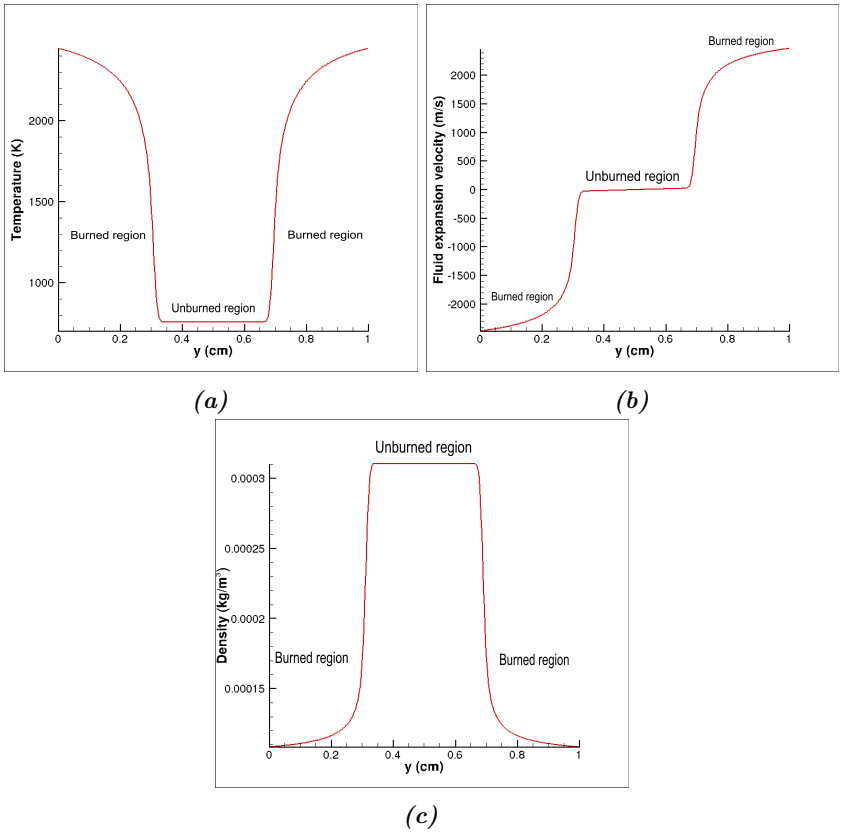

Figure 2.1: Temperature (a), fluid expansion velocity (b), and density (c) in a one dimensional simulation before the flame fronts meet. The left flame front is at $y = 0.32$ and the right is at $y = 0.68$ in these snapshots (approximetaly).

y-direction), expressed as:

$$\tau = \mu \frac{du}{dy}. \tag{2.2}$$

Flows are usually divided into laminar and turbulent flows[1] by the Reynolds number. A very low Re implies viscous creeping flow (inertia effects are negligible), moderate Re indicates a smoothly varying laminar flow, and a high Re indicates turbulent flow. A turbulent flow has slow variations in the time-mean, but has superimposed strong random high-frequency fluctuations. The randomness of turbulent flow makes it by far the hardest to numerically simulate. Both the mean flow and the fluctuations has to be solved and the resolution has to include all the turbulent scales.

Laminar (streamline) flow occurs when a fluid flows in parallel layers, with no disruption between the layers (Batchelor [4]). In laminar flow the particles moves orderly and there are no cross currents perpendicular to the direction of flow, nor eddies or swirl of fluids. One can also characterize laminar flow by high momentum diffusion and low momentum convection.

Turbulent flows are the most common in nature and engineering applications. Boundary layers growing on an airplane wing, flow of water in rivers, wakes of ships and water currents below the surface of the oceans, are all turbulent flows. Turbulent flow is characterized by its irregularity, diffusivity, large Reynolds number, three dimensional vorticity fluctuations and dissipation. A deterministic approach to turbulence is difficult, due to its irregularity (randomness), and one therefore often rely on statistical methods when dealing with turbulence phenomenas. Tennekes and Lumley [40] describes the diffusivity of turbulence as "the single most important feature as far as applications are concerned: it prevents boundary-layer separation on airfoils at large (but not too large) angles of attack, it increases heat transfer rates in machinery of all kinds, it is the source of the resistance of flow in pipelines, and it increases momentum transfer between winds and ocean currents". Turbulence often originates as an instability of laminar flows. The interaction of viscous terms and non-linear inertia terms in the equations of motion account for the instabilities. As turbulence is characterized by high levels of fluctuating vorticity (and is three dimensional and rotational), vorticity dynamics are very important for turbulent flows. Two dimensional velocity fluctuations could not maintain the random vorticity fluctuations. Lastly, turbulent flows are always dissipative. Deformation work is done by the viscous shear stress, something which increases the internal energy of the fluid at the

[1] There are more subcategories, but these are of less importance in this thesis.

expense of kinetic energy (of the turbulence). This implies that turbulence is dependent on a continuous supply of energy (Tennekes and Lumley [40]).

2.2 Combustion

Combustion is something most can relate to. Burning of wood, gas, oil, coal, etc. (fuels) are all well known combustion processes. Combustion is defined as "rapid oxidation generating heat, or both light and heat; also, slow oxidation accompanied by relatively little heat and no light" by Turns [41]. Most practical combustion devices, like the gas turbine, utilizes rapid oxidation. Usually combustion refer to an exothermic reaction involving a fuel and an oxidizer. In most combustion processes the oxidizer is air, due to it's availability and properties. Other oxidizers may be fluorine, ozone, chlorine, etc. For combustion to occur the fuel and oxidizer has to be mixed at molecular level, and there has to be a high enough temperature for the reaction to occur. Combustion can occur in either flame or non-flame mode, where a flame is defined as "a self-sustaining propagation of a localized combusion zone at subsonic velocities" (Turns [41, Ch. 8]). The flame itself is divided into two zones. The preheat zone, where little heat is released, and the reaction zone, where most of the chemical energy is released. The reaction zone is often divided further for convenience sake. It is then divided into a thin region of very fast chemistry, followed by a much wider region of slow chemistry. In the thin region the burning (destruction) of the fuel molecules takes place, and intermediate species form. As the region is so thin, temperature and concentration gradients are very large. These gradients actually provide the driving force for the flame to be self-sustaining. The wider region is dominated by radical recombination, a much slower process.

Flames are categorized into premixed and non-premixed (diffusion) flames. The difference between the two relates to the state of mixedness of the reactants. For a premixed flame the fuel and oxidizer are mixed at molecular level before the combustion. In a non-premixed flame the reactants are initially separated and the combustion takes place at the interface between the fuel and oxidizer. Flames can be further divided into laminar and turbulent flames.

2.2.1 Premixed Combustion

In a premixed flame the fuel and oxidizer is mixed before combustion. To characterize the mixture of fuel and oxidizer, the fuel equivalence ratio, ϕ, is

introduced:

$$\phi = \frac{(m_{\text{fuel}}/m_{\text{ox}})}{(m_{\text{fuel}}/m_{\text{ox}})_{\text{st}}}, \tag{2.3}$$

where m_{ox} is the amount of oxidizer, m_{fuel} the amount of fuel, and the subscript st denotes stoichiometric conditions. The stoichiometric quantity of oxidizer is the exact quantity needed to completely burn a quantity of fuel. If this is the case the fuel equivalence ratio will then be equal to one, $\phi = 1$, called a stoichiometric mixture. A lean (fuel-lean) mixture will be when there is more oxidizer than needed to completely burn the fuel, and thereby $\phi < 1$. A rich (fuel-rich) mixture gives the opposite, namely $\phi > 1$, as there is an excess of fuel. Often the fuel equivalence ratio will be the single most important factor in a combustion process to determine a system's performance.

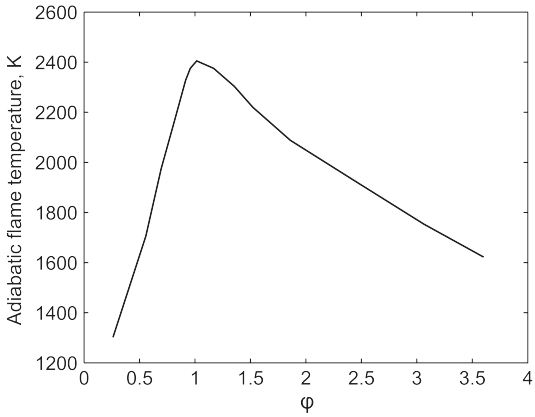

Figure 2.2: Adiabatic flame temperature for hydrogen-air mixtures (Drell and Belles [12]).

In fig. 2.2 the adiabatic flame temperature of hydrogen-air mixtures for different values of ϕ is presented. The flame temperature depend on the heat combustion and heat capacity (enthalpy) of the reactants and products. Through the energy equation for the combustion system the fuel equivalence ratio is then linked to the flame temperature (Turns [41]).

A premixed flame is characterized by the fundamental property of its "ability to propagate normal to itself with a burning velocity that, to first approximation, depends on thermo-chemical parameters of the premixed gas ahead of the flame alone" (Peters [30, Lecture 8]).

When intense combustion within small volumes is required, premixed flames are used. This includes spark ignition engines, industrial gas burners, stationary gas turbine engines and household appliances.

Flame Speed

The flame speed is considered as one of the most important characteristics in premixed combustion. Important flame stability characteristics such as liftoff and flashback (see section 2.2.4), and the flame shape are dictated by the flame speed.

The laminar flame speed, S_L, is defined as the speed at which an observer riding the flame would experience the unburned mixture approaching at (Turns [41, Ch. 8]). The laminar flame speed is a property of the thermal and chemical properties of the mixture alone and is defined as:

$$S_L = \frac{\dot{m}''}{\rho_u}, \tag{2.4}$$

where $\dot{m}''$ is the reactant mass flux and ρ_u is the unburned gas density. This definition follows from a simple consideration of

$$\rho_u S_L A \equiv \rho_u v_u A = \rho_b v_b A, \tag{2.5}$$

which is the contiunity equation, where ρ_u is the density of the unburned reactants, $S_L = v_u$ is the laminar flame velocity, A is the area of the flame front, ρ_b is the density of the burned products and v_b is the speed of the burned products. The velocity of the products has to be higher than the velocity of the reactants due to the lowering of density (temperature increase) over the flame.

The laminar flame speed is strongly dependent on temperature (in a fuel-air mixture). This relates to the fact that the reaction rate is an exponential function of the temperature. Increasing temperature in the unburned gas (or surroundings) then leads to an increased flame speed. The laminar flame speed is also dependent on the pressure and fuel equivalence ratio. With increasing pressure the flame speed will decrease. The fuel equivalence ratio affects the flame speed by affecting the flame temperature. An expression for the order of the laminar flame speeds dependency on pressure and temperature is developed in Turns [41, Eq. 8.29]:

$$S_L \propto \bar{T}^{0.375} T_u T_b^{-n/2} \exp(-E_A/2R_u T_b) P^{(n-2)/2}, \tag{2.6}$$

where $\bar{T} \equiv 0.5(T_b + T_u)$, n is the overall reaction order, T_b and T_u are the burned and unburned temperatures, respectively, E_A is the activation energy, R_u is the

universal gas constant, and P is the pressure. As the global reaction order for hydrocarbons are about two ($n = 2$), the temperature dependence discussed earlier is apparent, but the flame speed should be independent of pressure. The reaction order for hydrogen-air combustion is however found to be less than two for fuel equivalence ratios in the interval 0.56-3 and pressures up to 10 MPa in a previous work (Agnew and Graiff [3]). In fig. 2.3 the effects of equivalence ratio and temperature on laminar burning velocity in hydrogen-air mixtures are presented.

The order of a reaction is how many concentrations the reaction rate is dependent on. This means that an order of one is a uni-molecular reaction (or a dissociation). Order two is a regular bi-molecular reaction and order three covers the reaction between three molecules (this is uncommon, but is typically the reactions involving third bodies). The overall order is then the comprised order for the whole mechanism (all the elementary reactions).

A turbulent flame has a flame speed that depends on the character of the flow and on the mixture properties (Turns [41, Ch. 12]). It is defined as the velocity at which unburned mixture enters the flame zone in a direction normal to the flame front. The turbulent flame speed can be expressed as:

$$S_t = \frac{\dot{m}}{\bar{\mathrm{A}}\rho_u}, \tag{2.7}$$

where $\dot{m}$ is the reactant flow rate, ρ_u the unburned gas density and $\bar{\mathrm{A}}$ the time-smoothed flame area.

In fig. 2.4 the effect of equicalence ratio, unburned gas temperature, and pressure and turbulence intensity on the ratio of turbulent to laminar flame speed is presented.

Experimental data show some interesting correlations for the flame speed and its dependency on pressure. Generally a negative dependence on pressure for hydrocarbon fuels and hydrogen with respect to laminar flame speed is seen (Qin et al. [32], Turns [41], Heravi et al. [19]). For turbulent flame speeds the opposite trend has been observed (Lipatnikov and Chomiak [26]).

Flame Thickness

The flame thickness, δ_f, can be defined from the temperature profile of the flame. Then the flame thickness can be defined as the distance from the unburned temperature, T_u, to the burned temperature, T_b. For a simple flame where the temperature profile is assumed to be linear the flame thickness can be found

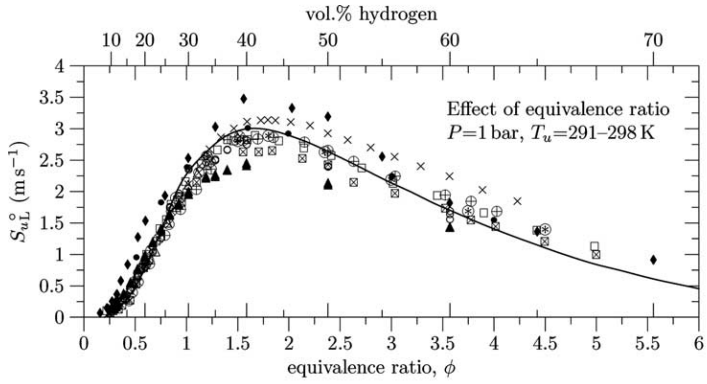

(a) Laminar burning velocity versus equivalence ratio.

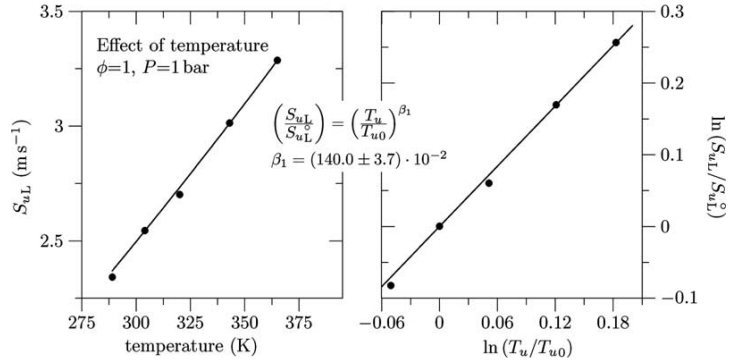

(b) Laminar burning velocity versus temperature.

Figure 2.3: Effect of equivalence ratio (upper part) and temperature (lower-left) on the laminar burning velocity of hydrogen-air mixtures (Dahoe [8]).

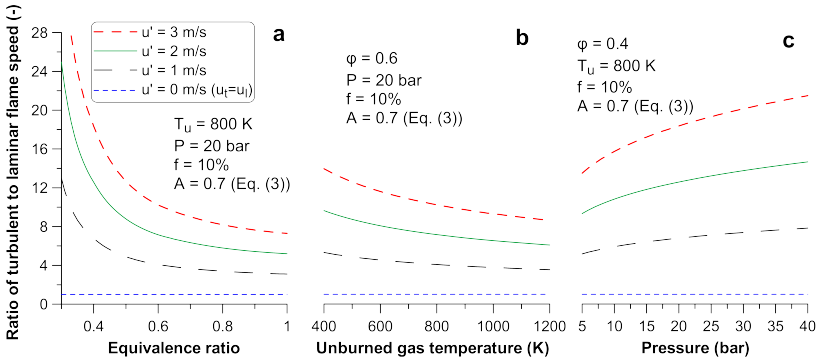

Figure 2.4: Effect of (a): equivalence ratio, (b): unburned gas temperature, and (c): pressure and turbulence intensity, on the ratio of turbulent to laminar flame speed under engine-relevant conditions (Rakopoulos et al. [33]).

using the expression (Turns [41, Eq. 8.21b]):

$$\delta_f = \frac{2\alpha}{S_L}, \tag{2.8}$$

where $\alpha \equiv \frac{k}{\rho_u c_p}$ is the thermal diffusivity.

An expression for the flame thickness order of dependency on temperature and pressure is developed in Turns [41, Eq. 8.30]:

$$\delta_f = \bar{T}^{0.375} T_b^{n/2} \exp(E_A/2R_u T_b) P^{-n/2}. \tag{2.9}$$

Again for hydrocarbons n are about two. With increasing temperature or pressure the flame thickness will then decrease according to the relation given.

Heravi et al. [19] gives an equation for measuring the flame thickness:

$$\delta_f = \frac{T_b - T_u}{max\left(\left|\frac{\partial T}{\partial x}\right|\right)}, \tag{2.10}$$

(which gives a good approximation).

The flame thickness is important in numerical computations as the flame has to be resolved by the computations. This gives a constraint for the spatial resolution as the flame needs a sufficient number of grid points to be considered resolved.

2.2.2 Non-Premixed Combustion

In non-premixed (diffusion) combustion there is no air mixed with the fuel before the combustion process. While the combustion occurs the fuel is mixing with the surrounding air by convection and diffusion. Fuel and oxidizer has to be mixed at molecular level for the chemical reactions to occur. In combustion, diffusion is usually the rate limiting step as the combustion is much faster than the diffusion. As the diffusion then basically controls the entire process, the reason for naming it diffusion flames makes sense (Peters [30]). Due to the fact that the mixing process is slower than the chemical reactions, and thus limits the burning rate, a good flame stability can be obtained.

The necessary gradients in non-premixed flame propagation are sustained by the chemical reaction. In non-premixed flames, due to the gradients, fuel and oxidizer diffuse to the flame front. The flame is fixed to the interface between fuel and oxidizer and the product species and energy is then diffused away from the flame zone (Warnatz et al. [43, Ch. 9]).

Non-premixed flames are utilized in large combustion devices, such as furnaces. Other examples are diesel engines, aircraft gas turbines and steam boilers. To premix large amounts of fuel and oxidizer involves a serious safety problem (Peters [30]). Combustion is often partially premixed to have better control over flame stability and pollutant emissions, like in gas boilers or jet engine combustion chambers (Peters [30]).

2.2.3 The Preferential Diffusion Effect

An important process in combustion is the preferential diffusion effect. In short the higher diffusive reactants move towards the flame front faster than the lower diffusive reactants in the reaction zone of a turbulent flame. This can create a bulge in the flame front, as the higher diffusive reactants will move into the unburned gas more rapidly.

For fuels where the diffusion coefficient is higher than that of oxygen and nitrogen, as it is for hydrogen, the fuel will diffuse into the convex part of the flame, towards the unburned gas. This can cause a local increase in the fuel equivalence ratio, which in turn can affect the whole domain, and uncorrect prediction of the emissions (soot, etc.). The local flame speed may change due to this effect.

A frequently invoked assumption is the *unity* Lewis number *assumption* which is a great simplification. The Lewis number, Le, is defined as:

$$\mathrm{Le} = \frac{\alpha}{D}, \tag{2.11}$$

where α is the thermal diffusivity and D is the mass diffusivity. Every chemical species has a Lewis number. For hydrogen this is not equal to unity and for hydrogen-air mixtures Le varies extensively with ϕ due to the high molecular diffusivity of hydrogen (Turns [41]).

2.2.4 Flame Stabilization

In turbulent combustion flame stabilization plays a major role concerning safety, efficiency and emissions. In Turns [41, Ch. 12] a stable flame is defined as "a flame that is anchored at a desired location and is resistent to flashback, liftoff and blowout over the operating range of the device".

The phenomena of flashback is when the flame propagates upstream of the desired flame location. This may occur when the local flame speed is larger than the mean flow velocity. For a premixed combustion flashback implies that the flame may propagate into the mixing zone, which is in no way desired.

When the flame is not anchored at the burner tube or port, but is stabilized at some distance from the port, the condition is called lift-off. The flame and burner become separated, something which can cause several problems like delayed ignition, loss of flame and failed ignition.

Keywords for flame stabilization is then to have good control over local ignition, flame propagation, extinction and re-ignition in order to obtain a system where the local turbulent flame speed matches the local mean velocity (Turns [41, Ch 8]).

2.3 Hydrogen Fundamentals

Hydrogen, H_2, is the lightest molecule there is and it does have some interesting properties compared to other fuels. Hydrogen combustion is carbon-free (no soot due to this), and its only pollutant is NO_x. In table 2.1 the properties of hydrogen is compared with methane and iso-octane. Methane and iso-octane are supposed to represent natural gas and gasoline, respectively. The properties of hydrogen has its advantages and its downsides. The fact that hydrogen combustion generates virtually zero harmful emissions (one of course have to consider the NO_x emissions) and has a potentially high efficiency (Verhelst and Wallner [42]), are two points strongly in favor of hydrogen combustion.

As one can see from table 2.1, as well as being light, relative to methane and iso-octane, it has a low density, high diffusivity, low minimum ignition energy, short minimum quenching distance, a large flammability range, high lower and higher heating value, and a very high energy-to-weight ratio.

Table 2.1: Hydrogen properties compared with methane and iso-octane at 300 K and 1 atm (Verhelst and Wallner [42]).

Property	Hydrogen	Methane	Iso-octane
Molecular weight (g/mol)	2.016	16.043	114.236
Density (kg/m^3)	0.08	0.65	692
Mass diffusivity in air (cm^2/s)	0.61	0.16	∼0.07
Minimum ignition energy (mJ)	0.02	0.28	0.28
Minimum quenching distance (mm)	0.64	2.03	3.5
Flammability limits in air (vol%)	4-75	5-15	1.1-6
Flammability limits, ϕ	10-0.14	2-0.6	1.51-0.26
Lower heating value (MJ/kg)	120	50	44.3
Higher heating value (MJ/kg)	142	55.5	47.8
Stoichiometric air-to-fuel ratio (kg/kg)	34.2	17.1	15.0
Stoichiometric air-to-fuel ratio (kmol/kmol)	2.387	9.547	59.666

In table 2.2 the properties of hydrogen-air, methane-air and iso-octane-air mixtures at 300 K, 1 atm and stoichiometric conditions are listed. Worth noting is the relatively high autoignition temperature and high laminar flame speed of hydrogen at atmospheric conditions compared to other fuels. While the combustion characteristics of hydrogen allow clean and efficient operation at low engine loads, it presents difficulties at high engine loads. According to White et al. [44] "the low ignition energies of hydrogen-air mixtures cause frequent unscheduled combustion events, and high combustion temperatures of mixtures closer to the stoichiometric composition lead to increased NO_x production". This limits the power density of hydrogen combustion.

The global reaction mechanism between H_2 and O_2 is given by

$$2H_2 + O_2 \rightarrow 2H_2O, \tag{2.12}$$

with a global reaction rate

$$\frac{d\left[X_{H_2}\right]}{dt} = -k_G(T)\left[X_{H_2}\right]^n\left[X_{O_2}\right]^m, \tag{2.13}$$

where $[X_i]$ is the molar concentration of the ith species, k_G is the global rate coefficient, and the exponents n and m relate to the reaction order. The global rate coefficient k_G can be expressed through the empirical Arrhenius form (if the temperature range of interest is not too great):

$$k_G = B_0 \exp(-E_A/R_uT), \tag{2.14a}$$

Table 2.2: Mixture properties for hydrogen-air, methane-air and iso-octane-air at 300 K, 1 atm and stoichiometric mixture ($\phi = 1$) (Verhelst and Wallner [42]).

Property	H_2-air	CH_4-air	C_8H_{18}-air
Volume fraction fuel (%)	29.5	9.5	1.65
Mixture density (kg/m^3)	0.850	1.123	1.229
Kinematic viscosity (mm^2/s)	21.6	16	15.2
Autoignition temperature (K)	858	813	690
Adiabatic flame temperature (K)	2390	2226	2276
Thermal conductivity (10^{-2}W/mK)	4.97	2.42	2.36
Thermal diffusivity (mm^2/s)	42.1	20.1	18.3
Laminar flame speed, ~ 360 K (cm/s)	290	48	45

where B_0 is a constant termed the pre-exponential factor. Or it can be expressed by the three parameter form

$$k_G = B_0 T^b \exp(-E_A/R_u T), \tag{2.14b}$$

where B_0, b and E_A are three empirical parameters.

This system may look fairly comprehensible, but the picture is a bit more complex. In the reaction between H_2 and O_2 there are a lot of elementary reactions. There is no simple path from fuel to product. There are a number of elementary reactions involving many intermediate species. An intermediate species is a molecular entity formed from the reactants which reacts further to give the directly observed products of a chemical reaction. That is, it is neither a product nor a reactant. An elementary reaction is a chemical reaction where one or more of the chemical species react directly to form products in a single reaction step and with a single transition state. The collection of elementary reactions necessary is called a reaction mechanism.

In a multistep reaction mechanism the rate of reaction is based on all the elementary reactions:

$$\mathrm{H} + \mathrm{O_2} \underset{\mathrm{k_{f1}}}{\overset{\mathrm{k_{r1}}}{\Leftrightarrows}} \mathrm{O} + \mathrm{OH}, \tag{2.15a}$$

$$\mathrm{O} + \mathrm{H_2} \underset{\mathrm{k_{f2}}}{\overset{\mathrm{k_{r2}}}{\Leftrightarrows}} \mathrm{H} + \mathrm{OH}, \tag{2.15b}$$

$$\mathrm{H_2} + \mathrm{OH} \underset{\mathrm{k_{f3}}}{\overset{\mathrm{k_{r3}}}{\Leftrightarrows}} \mathrm{H_2O} + \mathrm{H}, \tag{2.15c}$$

$$\mathrm{O} + \mathrm{H_2O} \underset{\mathrm{k_{f4}}}{\overset{\mathrm{k_{r4}}}{\Leftrightarrow}} \mathrm{OH} + \mathrm{OH}, \tag{2.15d}$$

$$\vdots$$

where k_r and k_f are rate coefficients for the elementary reactions. Then the reaction rate has to be described for each elementary reaction, which yields a system of first-order ordinary differential equations. These equations describe the evolution of the chemical system starting from a given initial condition:

$$\frac{d\left[\mathrm{X}_i\right](t)}{dt} = f_i\left(\left[\mathrm{X}_1\right](t), \left[\mathrm{X}_2\right](t), \ldots, \left[\mathrm{X}_n\right](t)\right), \tag{2.16a}$$

with

$$\left[\mathrm{X}_i\right](0) = \left[\mathrm{X}_i\right]_0. \tag{2.16b}$$

When using a simple chemistry representation there is only one elementary reaction and only the global rate coefficient has to be modeled. When one uses a detailed chemistry representation a number of elementary reactions are involved. This implies a lot more modeling (each elementary reaction has to be modeled). However, for a simple chemistry representation the global rate coefficient has to be tuned according to each case (set for a specific range), while a detailed chemistry representation takes into account the variation of for instance the fuel equivalence ratio.

In table 2.3 a reaction mechanism for hydrogen and oxygen by Li et al. [24] is presented. In this mechanism there is a total of nineteen elementary reactions which have to satisfy the balanced global reaction. This model is chosen as it is comprehensively tested experimentally and shows good agreement. Ströhle and Myhrvold [36] suggests that this reaction mechanism is the best suited for hydrogen-air chemistry.

Table 2.3: Detailed H_2/O_2 reaction mechanism from Li et al. [24].

n	Reaction
1	$H + O_2 \Leftrightarrow O + OH$
2	$O + H_2 \Leftrightarrow H + OH$
3	$H_2 + OH \Leftrightarrow H_2O + H$
4	$O + H_2O \Leftrightarrow OH + OH$
5	$H_2 + M \Leftrightarrow H + H + M$
6	$O + O + M \Leftrightarrow O_2 + M$
7	$O + H + M \Leftrightarrow OH + M$
8	$H + OH + M \Leftrightarrow H_2O + M$
9	$H + O_2 + M \Leftrightarrow HO_2 + M$
10	$HO_2 + H \Leftrightarrow H_2 + O_2$
11	$HO_2 + H \Leftrightarrow OH + OH$
12	$HO_2 + O \Leftrightarrow OH + O_2$
13	$HO_2 + OH \Leftrightarrow H_2O + O_2$
14	$HO_2 + HO_2 \Leftrightarrow H_2O_2 + O_2$
15	$H_2O_2 + M \Leftrightarrow OH + OH + M$
16	$H_2O_2 + H \Leftrightarrow H_2O + OH$
17	$H_2O_2 + H \Leftrightarrow H_2 + HO_2$
18	$H_2O_2 + O \Leftrightarrow OH + HO_2$
19	$H_2O_2 + OH \Leftrightarrow H_2O + HO_2$

* M is a third body - a molecule that does not change the chemical composition of the reaction, but participates by "receiving" and "giving away" energy.

2.4 Thermoacoustic Oscillations

Thermoacoustic oscillations can occur whenever combustion or heat exchange is done in an acoustic resonator (Keller and McLaughlin [22]). They may occur in many different devices, such as rockets, ramjets, gas boilers and aeroengines. The concern of this thesis is with stationary gas turbines and premixed combustion. For premixed combustion almost all air enters through the burner. This means that there is almost no sound attenuation downstream of the primary zone of combustion. In a conventional gas turbine the liners are effective sound attenuators, as a substantial percentage of air enter downstream of the primary zone of combustion. The problems with stabilization of the flame in premixed combustion and the attenuation problems has made thermoacoustic stability into an important issue in modern gas turbine development (Keller and McLaughlin [22]).

Lean premixed combustion are unfortunately susceptible to combustion instability. This is a generic problem, which of course is unwanted. When one burn lean and premixed, any velocity variation of air supplied to the combustion chamber leads to large variations in the instantaneous rate of heat release (Dowling and Hubbard [11]).

Thermoacoustic oscillations occur because unsteady heating generates sound waves, which produce pressure and velocity fluctuations. When the unsteady rate of heat input is in phase with the pressure perturbations, the acoustic waves gain energy. The amplitude of the pressure waves are in practice limited by non-linear effects, but may still cause structural damage (Dowling [10]).

The oscillations are divided into two categories: Self-excited and forced oscillations. An example of self-excited oscillations is acoustic radiation and dissipation generated by a boundary or shear layer. These are proportional to the square of the amplitude of an acoustic oscillation. The amplitude of self-excited oscillations are always limited by non-linearity (Keller [23]). Self-excited oscillations are difficult to investigate due to the non-linearity of the acoustic wave motion in the confined (or semi-confined) gas (Keller and McLaughlin [22]).

Kato et al. [21] studied “the effect of flame position and its spatial variation on prediction accuracy of combustion in a dry low emission (DLE) combustor”. They used a one-dimensional linear model to analyze the problem. It is found that “stability boundaries as well as frequencies of combustion oscillation can be predicted with higher accuracy when spatial distribution of heat release is accounted for”.

2.5 Governing Equations

The continuity, momentum, energy and transport of unburned mass fraction equations has to be solved to get a solution related to reactive flows.

The governing equations are presented for a one dimensional domain and an irreversible single step reaction, as the analytical approach (see section 4) is performed in one dimension. The governing equations are given in the same form as Talei et al. [37], with spatial coordinate ζ:

$$\frac{\partial \rho}{\partial t} + \frac{1}{\zeta^a}\frac{\partial \zeta^a \rho u}{\partial \zeta} = 0, \tag{2.17}$$

$$\frac{\partial \rho u}{\partial t} + \frac{1}{\zeta^a}\frac{\partial \zeta^a \rho u^2}{\partial \zeta} + \frac{\partial P}{\partial \zeta} = \frac{1}{\zeta^a}\frac{\partial \zeta^a \tau_{\zeta\zeta}}{\partial \zeta} - a\tau_{\phi\phi}/\zeta, \tag{2.18}$$

$$\frac{\rho e_t}{\partial t} + \frac{1}{\zeta^a}\frac{\partial}{\partial \zeta}\left[\zeta^a \left(\rho e_t + P\right) u\right] = \frac{1}{\zeta^a}\frac{\partial}{\partial \zeta}\left(\zeta^a u \tau_{\zeta\zeta}\right) - \frac{1}{\zeta^a}\frac{\partial}{\partial \zeta}\left(\zeta^a q\right) + Q\dot{\omega}, \tag{2.19}$$

$$\frac{\partial \rho Y}{\partial t} + \frac{1}{\zeta^a}\frac{\partial}{\partial \zeta}\left(\zeta^a \rho Y u\right) = \frac{1}{\zeta^a}\frac{\partial}{\partial \zeta}\left(\zeta^a \rho D \frac{\partial Y}{\partial \zeta}\right) - \dot{\omega}, \tag{2.20}$$

where ρ is the density, u is the velocity, P is the pressure, $\tau_{\zeta\zeta}$ and $\tau_{\phi\phi}$ are the stress tensors, q is the heat flux, e_t is the specific total internal energy, Y is the unburned fuel mass fraction, D is the mass diffusion coefficient, $\dot{\omega}$ is the chemical reaction rate, Q is the specific heat of reaction and t is the time. For the three configurations in this thesis (planar, axisymmetric and spherically symmetric) the variables a and ζ are defined as follows:

$$a = 0, \quad \zeta = x, \quad \text{planar},$$

$$a = 1, \quad \zeta = r, \quad \text{axisymmetric},$$

$$a = 2, \quad \zeta = R, \quad \text{spherically symmetric},$$

The total specific internal energy, pressure, heat flux, stress tensors, specific heat of reaction and the reaction rate are expressed as follows:

$$e_t = \frac{1}{2}u^2 + \frac{p}{\rho\left(\gamma - 1\right)}, \tag{2.22}$$

$$p = \frac{\gamma - 1}{\gamma}\rho c_p T, \tag{2.23}$$

$$q = -k\frac{\partial T}{\partial \zeta}, \tag{2.24}$$

$$\tau_{\zeta\zeta} = \mu \left(2\frac{\partial u}{\partial \zeta} - \frac{2}{3}\frac{1}{\zeta^a}\frac{\partial \zeta^a u}{\partial \zeta} \right), \tag{2.25}$$

$$\tau_{\phi\phi} = \mu \left(2\frac{u}{\zeta} - \frac{2}{3}\frac{1}{\zeta^a}\frac{\partial \zeta^a u}{\partial \zeta} \right), \tag{2.26}$$

$$Q = c_p \left(T_b - T_u \right), \tag{2.27}$$

$$\dot{\omega} = \Lambda \rho Y \exp\left(\frac{-\beta \left(1 - \Theta\right)}{1 - \alpha \left(1 - \Theta\right)} \right), \tag{2.28}$$

where T is the temperature, c_p is the specific heat capacity at constant pressure, k is the thermal conductivity and μ is the dynamic viscosity of the gas, the subscripts u and b correspond with the unburned and burned gas, respectively, α and β are parameters determining the flame heat release and activation temperature, respectively (Poinsot and Veynante [31]),

$$\Theta = \left(T - T_u \right) / \left(T_b - T_u \right), \tag{2.29}$$

and

$$\Lambda = B_0 \exp\left(\frac{-\beta}{\alpha} \right). \tag{2.30}$$

Here B_0 is the pre-exponential factor and Θ is the reduced temperature.

3 Prior Work

DNS is mainly used in numerical studies where turbulence is a factor. In this study laminar flow will be investigated, but still DNS will be used as it is the most accurate tool for these kind of simulations. This is also due to possible direct comparison with later work.

Moin and Mahesh [27] describe DNS as "A tool in Turbulence Research". Their paper review DNS of non-reacting (no combustion) turbulent flows, and also gives insight into the general development of DNS and its usage. DNS is used mainly as a tool to verify turbulence models and to gain insight into turbulent phenomenas that would not be possible using experimental methods. Some examples of these numerical experiments are: Forced isotropic turbulence, the minimal channel, shear-free boundary layers and the interaction of turbulence with shock waves. They stress that over the years the "complexity of computed flows has noticeably increased, but that Reynolds numbers are still low". The trends in computer hardware development indicates that this will be the case in the foreseen future. The authors point out that "the greatest strength of DNS is the stringent control it allows over the flow being studied" and that DNS does not have to reach real-life Reynolds numbers to be useful in real-life applications.

Premixed combustion is (as mentioned in section 2.4) susceptible to combustion instabilities. The next paragraph therefore sums up some of the extensive research done in the field of thermoacoustic oscillations.

Keller and McLaughlin [22] presents an overview of thermoacoustic oscillations in gas turbine combustors with premixed combustion. They stress that as almost all the air enters through the burners in a modern premixing combustor, there will be almost no sound attenuation downstream of the primary zone of combustion. This together with the problem of stabilizing premixed flames, make thermoacoustic oscillations one of the most important issues in gas turbine combustor research. The paper discusses three thermoacoustic excitation mechanisms:

- Sound Generated by Entropy Nonuniformities.
- Sound Generated in the Primary Zone of Combustion: Self-Excited Oscillations.
- Sound Generated in the Primary Zone of Combustion: Forced Oscillations.

They conclude that there are two leading excitation mechanisms, namely periodic (lean) extinction and vortex rollup in the primary zone of the combustion. A

consideration of linear stability for a number of excitation mechanisms, lead to the conclusion that flow instabilities that produce fluctuations in the rate of reaction is the main cause of combustion-driven oscillations.

Dowling and Hubbard [11] uses a generalized acoustic equation to identify mechanisms driving combustion instability. The oscillations may lead to structural damage or increased heat transfer, which may in turn lead to overheating. A small unsteadiness in the rate of combustion generates sound, which gives pressure and velocity fluctuations. A lean and premixed combustion is especially sensitive to velocity variation of air supplied to the combustion chamber, since this will give large variations in the instantaneous rate of heat release. Dowling and Hubbard sums it up like this:

> "Instability is then possible because, while the acoustic waves perturb the combustion, the unsteady combustion generates yet more sound!"

The paper discusses influences on susceptibility to combustion oscillation and on the resonant frequency, something which is studied by a generic example of a premixed duct flame. The focus then turns onto lean premixed gas turbines. The article conclude that "as well as influencing the stability, the relationship between the unsteady rate of heat release and the flow affects the frequency of oscillation". The concept of turbulent flame speed is utilized to develop a kinematic flame model, which has proved useful to describe the unsteady heat release rate for totally premixed flames. It is however noted that the theory is simplified. Naturally the large-scale flow features may be observed, while smaller scale effects is not contained. This model was developed further to explain the features that cause unsteady combustion in a lean premixed combustor geometry. The largest source of unsteady combustion was identified as the change in flame surface area as changes in equivalence ratio alter the flame speed.

The next papers presented are only a selected few in the field of sound generation in combustion systems, and are chosen due to their informative nature and their resemblance with the topic of this thesis.

Guichard et al. [15] performed a two dimensional simulation of a turbulent V-shaped flame obtained by injecting a fully premixed mixture of fuel and oxidizer in a turbulent field. Non-reflecting boundary conditions were used in the spanwise direction, and the data used has been normalized. Figure 3.1 gives an impression of the interactions beween the thin flame front and the turbulent structures. It can be seen from fig. 3.2a that some turbulent structures in the fresh gas push on the reacting sheet. The flame propagation is illustrated in figs. 3.2b and 3.2d, where the two flame fronts meet face to face. This creates a pocket of fresh gas in the burned gases (fig. 3.2c) and a pressure wave will propagate from the area

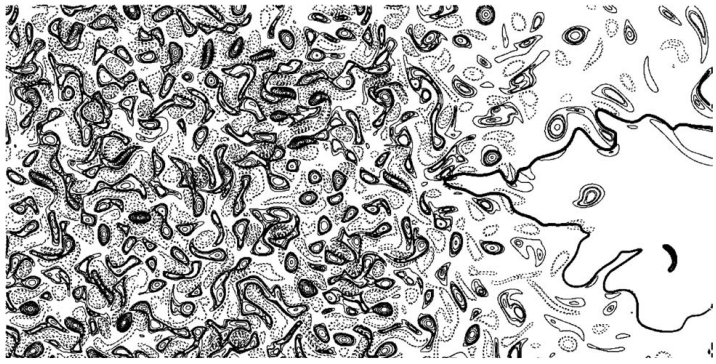

Figure 3.1: Snapshot of turbulent V-shaped flame (Guichard et al. [15, figure 15, p. 160]).

of the meeting flame fronts (fig. 3.2e). Figure 3.2 gives a good illustration of the phenomena of acoustic wave propagation. Guichard et al. however, does not expand on the topic of acoustic wave propagation.

Talei et al. [37] study the sound generated by premixed flame annihilation. They look at three cases: Planar, axisymmetric and spherically symmetric flame annihilation. Talei et al. use simple chemistry simulations, both for the flame dynamics and the acoustics. Their results show a significant increase in flame propagation velocity close to flame annihilation and that the amplitude of the far-field sound produced depends on the flame thickness. Based on Lighthill's acoustic analogy they present a theory that relates far-field sound to the flame annihilation event. This theory is then tested against the numerical results, showing an accurate agreement, if one only considers the temporal heat release in Lighthill's acoustic analogy. Talei et al. then try to simplify the problem. They assume an infinitely thin flame and constant flame speed. This approach gives a reasonably good prediction for the overall pressure change in the planar case, and significant under-prediction of the amplitude of the far-field sound produced for the axisymmetric and spherically symmetric case.

Talei et al. [38] build on this and look once again at the same three configurations: Planar, axisymmetric and spherically symmetric flame annihilation. They develop a theory to relate the pressure amplitude to the flame's propagation velocity and consumption speed. For unity Lewis number they get good agreement between theory and simulations. They also use Markstein's linear theory in an attempt to get a more practical approach. However, this leads

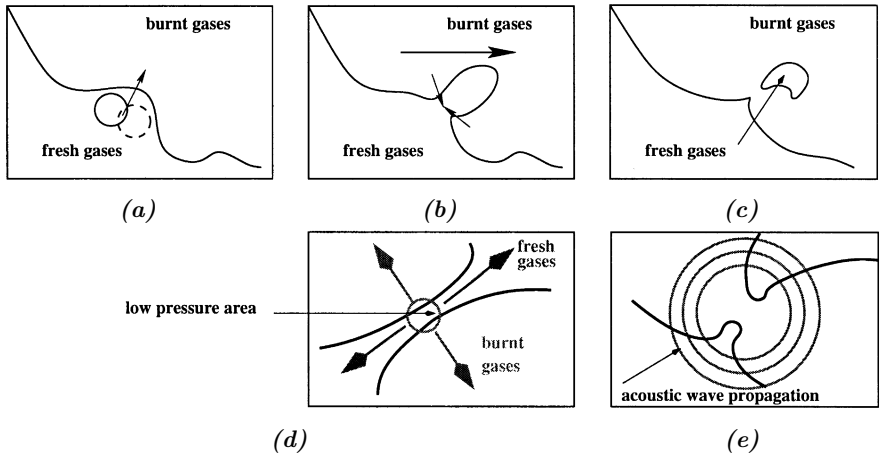

Figure 3.2: Sketch of the formation for a fresh gas pocket behind the flame front (Guichard et al. [15, figure 18, p. 162]).

to under-prediction of the radiated sound in the axisymmetric and spherical configurations, but is able to show the qualitative trends. Flames modeled with Lewis number other than unity is also investigated. Close to the annihilation event the flame either accelerate or decelerate, depending on the Lewis number. This is shown to affect the radiated sound significantly. The local consumption speed increases at flame annihiliation, leading to more sound produced compared with unity Lewis number. The opposite behaviour is observed for Lewis numbers less than unity.

Brear et al. [5] presents an analysis of the energy transported by disturbances in gaseous combustion. The paper extends the work of Myers [29], and introduces an extended form of Myers' 'disturbance energy'. An aeroacoustic DNS simulation of a forced, low-Mach-number, laminar, premixed flame is done, over which the disturbance energy budget is closed, to demonstrate that the volume integral of the disturbance energy source terms are directly related to the area-averaged far-field sound produced by a jet. By this method it is shown that several source terms are significant, also those involving the mean-flow and entropy. The authors then conclude "that the energetics of sound generation cannot be examined by considering the Rayleigh source term alone".

Talei et al. [39] in a later paper studies sound generation by two-dimensional laminar premixed flames. This is done with a DNS of low Mach number flames

with different Lewis numbers (0.5, 1 and 2) with a simple chemistry representation. The flame is excited by velocity perturbations at the inflow boundary for a range of frequencies. 'Flame pinch-off' and 'flame island burn-out' are observed as strong, monopolar sound sources at intermediate forcing frequencies for Lewis numbers 1 and 2. At Lewis number 0.5 almost no sound was produced. By using Dowling's reformulation of Lighthill's acoustic analogy the contribution of heat release rate fluctuations to the radiated sound is investigated. A flamelet model suggested by Clavin and Siggia [7] was used to get estimated values for comparison with the DNS result. The flamelet model assumes that heat release fluctuations are due to flame surface area fluctuations, and shows good agreement for unity Lewis number. However, for Lewis number 0.5 and 2 the pressure fluctuations due to heat release are over- and under-predicted, respectively. The authors suggest that the failure of the model in the non-unity Lewis number cases, as it is intended for turbulent flames and assumes a constant consumption speed along the surfaces, can be due to the "large modifications of the consumption speed where large surface area fluctuations is present".

These last four papers are of special interest as they deal with many of the same problems as this thesis will. They serve as valuable background information, and also as comparable datasets for this study. Simple chemistry representation has been used for these studies, and is consequently a motivation for comparing detailed chemistry representation DNS results with simple chemistry representation. This was done in the project work of fall 2012. Here it was found for fuel equivalence ratios 0.3, 0.5, 0.8 and 1.5 at $P = 1\,\text{atm}$ that the preferential diffusion has a larger impact in the case of simple chemistry representation. It was also found that with increasing fuel equivalence ratio the simple chemistry representation will yield a "thinner" flame.

4 Analytical Approach

In the project work done in the fall of 2012, an analytical study of the flame annihilation in one dimension was performed. The analytical problem solved can be visualized as a thin cylinder filled with hydrogen, which is then ignited at both ends (that is, a one dimensional planar flame, see fig. 5.1).

Some parts of the analytical study will be repeated here, as the resulting relations will be used in the results (for the full derivation of the relations, see appendix A). Also this section will give a good introduction to the various terms and variables investigated. The background and reasoning will be kept, while the derivation of the relations will be kept out and only the resulting relations will be given.

The study was based on eqs. (2.17) and (2.18) in one dimension in the planar case ($n = 0$ and $\zeta = x$). The continuity and momentum equations can then be written:

$$\frac{D\rho}{Dt} + \rho \nabla \cdot \vec{u} = 0, \tag{4.1}$$

$$\rho \left(\frac{\partial \vec{u}}{\partial t} + \vec{u} \cdot \nabla \vec{u} \right) = \rho \vec{g} - \nabla P + \nabla \cdot \underline{\tau}, \tag{4.2}$$

where $\frac{D}{Dt}$ is the substantial derivative, ρ the fluid density, t the time, ∇ the del operator, $\vec{u}$ the fluid velocity, $\vec{g}$ the gravitational acceleration, P the pressure, and $\underline{\tau}$ the stress tensor. The stress tensor is defined as:

$$\underline{\tau} = \mu \left(\nabla \vec{u} + (\nabla \vec{u})^T + \lambda \nabla \cdot \vec{u}\ I \right), \tag{4.3}$$

where μ is the dynamic viscosity, λ the second viscosity coefficient and I the identity matrix. These equations make out the basic equations needed to solve the system.

To be of practical use the equations are simplified using the following relations and assumptions: Viscous and gravity terms in eq. (4.2) is neglected, an isotherm process is assumed and the equations are written out with the spatial coordinate for one dimensional flow, namely x. Complete combustion (no unburned fuel) and simple chemistry (one-step) is assumed. The equations then reduces to:

$$\frac{\partial \rho}{\partial t} + \rho \frac{\partial u}{\partial x} + u \frac{\partial \rho}{\partial x} = 0, \tag{4.4}$$

$$\frac{\partial u}{\partial t} + u \frac{\partial u}{\partial x} + \frac{1}{\rho} \frac{\partial P}{\partial x} = 0. \tag{4.5}$$

It is desirable to model the terms in eqs. (4.4) and (4.5) with measurable data from the simulations. To do this the development of relevant equations is split into regions, before time of impact and after time of impact. Time of impact, from now on denoted as τ_i, is defined as the time when the temperature in the middle of the domain, x_{center}, changes from the initial temperature in the unburned domain.

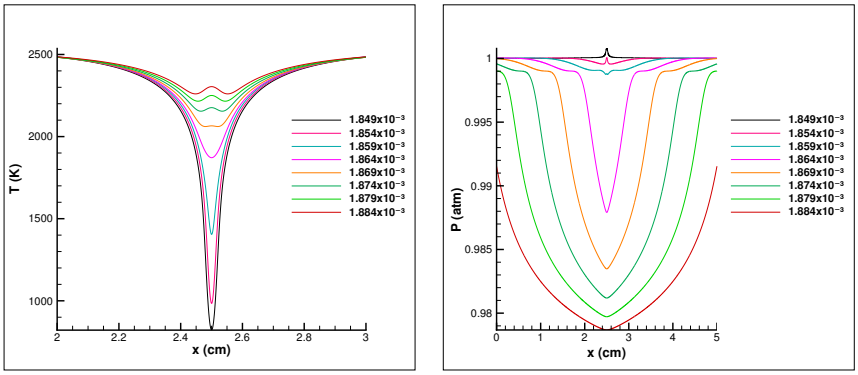

(a) Temperature as a function of position when $\phi = 1.5$.

(b) Pressure as a function of position when $\phi = 1.5$.

Figure 4.1: Temperature and pressure profiles from time of impact to time when minimum pressure is obtained.

Before time of impact the two flames are modeled as non-interacting, that is, two individual flames. This simplifies the problem as no interaction terms have to be considered. It is expected that there is a pressure difference between the burned and unburned region, which can be seen as the driving pressure for the problem. This pressure difference together with the fluid expansion velocity is modeled in the next section.

As the flames propagates towards each other, the temperature behind the flames (burned fuel) is much higher than the temperature in front of the flames (unburned fuel). The higher temperature leads to an expansion of the burned gases, which translates a significant drop in density. This triggers outflow from the domain. After time of impact the flames annihilate. When the flames annihilate the amount of fuel to sustain the expansion process diminishes, but the outwards velocity still has inertia. This process is expected to generate a pressure drop in the middle of the domain (where the flame annihilate), as the depletion

of fuel will lead to a severe density fall. One can think of it as taking energy from the pressure to be able to stop the fluid flow (as there is no more fluid to expand). A two dimensional DNS simulation by Andrea Gruber[2] indicate pressure waves moving out of the domain from the annihilating flames. The pressure difference between the surrounding domain and the maximum pressure drop due to annihilation is modeled. The frequency and amplitude of these waves are of special interest as this may help in identifying ways of avoiding dangerous resonance frequencies.

In fig. 4.1 the temperature and pressure profiles from time of impact until the time when the minimum pressure is obtained is presented. These plots are generated from the results of the DNS simulations done in one dimension and is given here as a visualization of the flame dynamics and physical effects of the annihilation event.

4.1 Modeling before time of impact

The time frame before τ_i is the first investigated. This is not the most exciting as it could have been done with one flame only, and it has been done many times before. It is however an important task to do this analysis to ensure that the simulations are correct according to available theory and other works. Before τ_i two relations will be uncovered; the pressure difference between the unburned and burned domain, ΔP, and the fluid expansion velocity, u_b.

For both before and after τ_i the equations will first be simplified and then discretized. The discretization uses a simple one step approach and looks only at the parameters in the steady unburned and burned region.

Pressure

Before τ_i there is a slightly higher pressure in the unburned region. This can be seen as the driving pressure of the flame fronts. To model the order of this pressure difference, the base equations have to be simplified. Before τ_i the two flames is assumed to not interact with each other, thus one need only to investigate one of the flames at this point.

In a coordinate system following one of the flame fronts, the following relation was found by some manipulation of eq. (4.5):

$$\Delta P = \rho \delta_f \frac{u_b}{\tau_f} = \rho S_L u_b, \tag{4.6}$$

[2]Personal communication.

where u_b is the fluid expansion velocity, $\tau_f = \frac{\delta_f}{S_L}$ is the time scale for the propagation of the flame front, δ_f is the width of the flame, and S_L is the flame propagation velocity.

Fluid expansion velocity
Before τ_i the temperature behind the flame is much higher than the temperature in front of the flame. This will lead to an expansion of the burned fuel out of the domain, as the density lowers. This velocity is called the fluid expansion velocity, u_b, and is thought to only be dependent on three parameters: the flame propagation velocity, S_L, the fluid density in a steady burned region behind the flame, ρ_b, and in the steady unburned region, ρ_u, i.e.:

$$u_b = f(S_L, \frac{\rho_b}{\rho_u}). \tag{4.7}$$

After some manipulations of eq. (4.4) the explicit expression for u_b then reads:

$$u_b = S_L \left(\frac{\rho_u}{\rho_b} - 1 \right). \tag{4.8}$$

It is noted that S_L comes from the relation $S_L = \frac{\delta_f}{\tau_f}$.

4.2 Modeling after time of impact

After τ_i the flames can no longer be treated as separate flames. This increases the complexity of the system. The same method of simplification and simple discretization is still used. After τ_i only one parameter will be investigated, namely the pressure difference between the initial pressure and the minimum pressure after τ_i.

Pressure
As the flames meet the temperature between them will increase. The pressure is then expected to drop as there is a rapid combustion with fuel spent, i.e. a lowering of the fuel fraction. The pressure drop will spread in the domain and move out of the domain as a pressure wave.

The relation between the pressure change and density, speed of sound and fluid expansion velocity is by manipulation of eq. (4.5) found to be:

$$\Delta P_{\min} = \rho u_p u_b. \tag{4.9}$$

It is noted that u_p is defined as $u_p = \frac{\delta_a}{\tau_a}$, where τ_a and δ_a are the time and length scale, respectively, based on the propagation of the pressure wave.

4.3 Other Studies

In Talei et al. [37] a theory is developed to describe the production of sound as a function of key flame parameters. They base their work on Lighthill [25] and the reformulated Lighthill's equation for combusting flows by Dowling [9]:

$$\begin{aligned}\frac{1}{C_\infty^2}\frac{\partial^2 P}{\partial t^2} - \nabla^2 p =& \frac{\partial}{\partial t}\left(\frac{\rho_\infty}{\rho}\left(\frac{Q\dot{\omega}}{c_p T} - \frac{\boldsymbol{\nabla}\cdot q}{c_p T} + \frac{\tau_{ij}}{c_p T}\frac{\partial u_i}{\partial x_j}\right)\right) \\ &+ \frac{\partial^2}{\partial x_i \partial x_j}\left(\rho u_i u_j - \tau_{ij}\right) \\ &+ \frac{1}{C_\infty^2}\frac{\partial}{\partial t}\left(\left(1 - \frac{\rho_\infty C_\infty^2}{\rho C^2}\right)\frac{\mathrm{D}p}{\mathrm{D}t} - \frac{P - P_\infty}{\rho}\frac{\mathrm{D}\rho}{\mathrm{D}t}\right) \\ &+ \frac{\partial^2}{\partial x_i \partial t}\left(u_i \rho_e\right), \end{aligned} \tag{4.10}$$

where the subscript ∞ refers to the flow variables in the far-field. In this report ρ_e is the excess density:

$$\rho_e = \rho - \rho_\infty - \left(P - P_\infty\right)/C_\infty^2. \tag{4.11}$$

In cases were the flow Mach number is low and combustion is unsteady, the first term on the right hand side in eq. (4.10) dominates the other terms (Dowling [9]). This term describes a strong monopolar source of sound (Strahle [35], Clavin and Siggia [7]). Talei et al. [37] only retains the source term associated with temporal fluctuations in the heat release, which leads to the following simplification of eq. (4.10):

$$\frac{1}{C_\infty^2}\frac{\partial^2 P}{\partial t^2} - \nabla^2 P = \frac{\partial}{\partial t}\left[\frac{\rho_\infty}{\rho}\left(\frac{Q\dot{\omega}}{c_p T}\right)\right]. \tag{4.12}$$

Equation (4.12) is modeled as a wave equation and with the approximation for small p'/p_u (i.e. low Mach number flows), where $p' = p - p_u$ is noted as the pressure in the far-field. The right hand side can then be expressed as:

$$\Pi(r,t) = \left(1 - \frac{T_u}{T_b}\right)\frac{\partial}{\partial t}\left(\dot{\omega}\left(r,t\right)\right). \tag{4.13}$$

In figs. 4.2 and 4.3 some of the results from Talei et al. [37] are given. Figure 4.2 compares simulations with eq. (4.12), and fig. 4.3 gives the pressure development after the annihilation event. It is noted that the pressure drop after τ_i is largest for the planar case, and smallest for the spherically symmetric case.

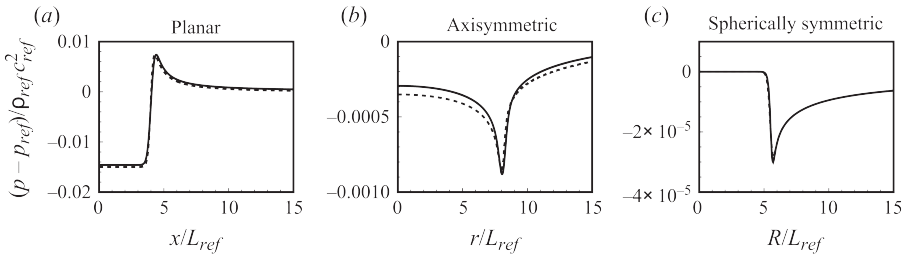

Figure 4.2: Non-dimensional pressure for the planar, axisymmetric and spherically symmetric flame annihilation from simulations (solid line), and solution of eq. (4.12) (dashed), $\delta/L_{ref} = 0.1$ (Talei et al. [37]).

Talei et al. [37] simplifies the problem further to get explicit expresions for the pressure in the far-field. First they look at flames of finite thickness. For planar flame annihilation they develop the following expression for the steady state far-field pressure:

$$P'(x,t) = -\rho_u c_b \left(1 - \frac{T_u}{T_b}\right) S_L, \tag{4.14}$$

where c_b is the sonic velocity.

In the axisymmetric flame annihilation event a complicated general solution is obtained by using the Heaviside function:

$$\begin{aligned} P'(r,t) = &-\rho_u \left(1 - \frac{T_u}{T_b}\right) S_L^2 H(t - r/c_b) \left\{ \ln\left(\frac{r/c_b}{t - \sqrt{t^2 - r^2/c_b^2}}\right) \right. \\ &\left. + H\left[c_b(t-\tau_1) - r\right] \ln\left(\frac{t - \tau_1 - \sqrt{(t-\tau_1)^2 - r^2/c_b^2}}{r/c_b}\right) \right\} \\ &+ \left(1 - \frac{T_u}{T_b}\right) \int_{\tau_1}^{t - r/c_b} \int_0^{\zeta^+} \frac{\zeta \partial\dot{\omega}/\partial\tau}{\sqrt{(t-\tau)^2 - r^2/c_b^2}} \mathrm{d}\zeta \mathrm{d}\tau. \end{aligned} \tag{4.15}$$

This general solution is expected to be valid as long as τ_1 is chosen such that the flame is sufficiently far from the origin. This result is hard to compare with numerical data due to the complexity of the formula.

In this study the pressure in the far-field found for flames of finite thickness under planar flame annihilation in eq. (4.14) is the most interesting. This is both

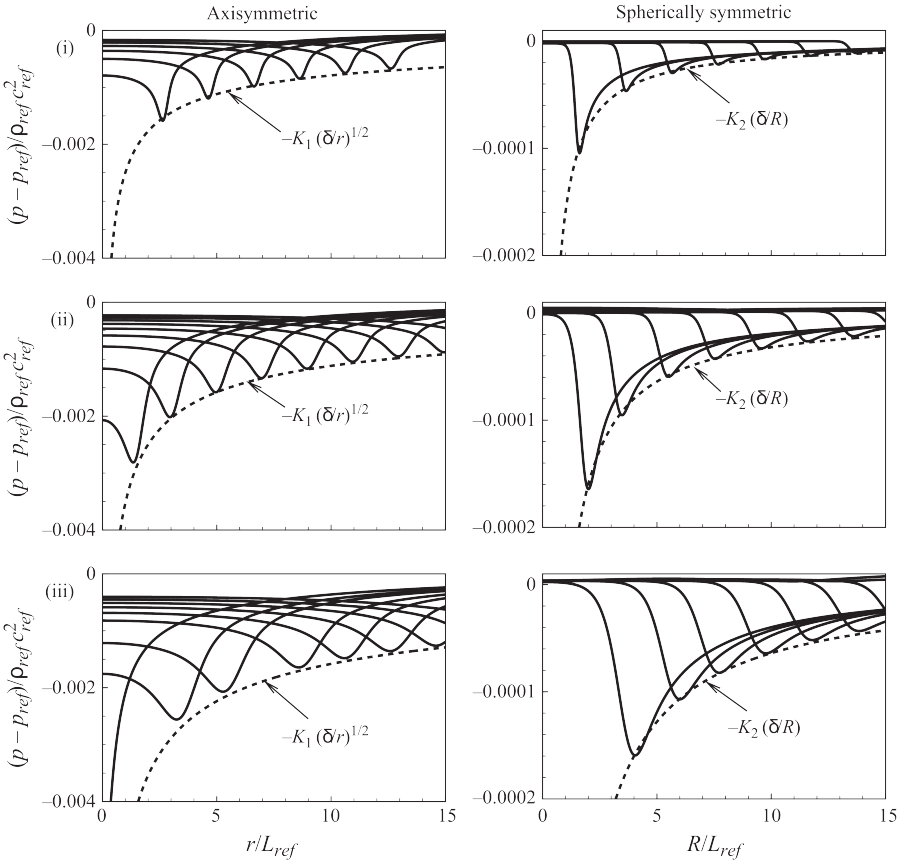

Figure 4.3: Non-dimensional pressure versus radius after the annihilation event for several time instants and different flame thicknesses: (i) $\delta/L_{ref} = 0.1$, (ii) $\delta/L_{ref} = 0.2$ and (iii) $\delta/L_{ref} = 0.4$ (Talei et al. [37]).

due to the simplicity of this formula and the fact that in this paper an analytical approach has only been done in one dimension for planar flame annihilation. The equation developed for the pressure difference after time of impact (eq. (4.9)) and the far-field pressure from Talei et al. [37] are repeated for the sake of overview:

$$\Delta P_{\min} = \rho u_p u_b,$$

$$P'(x,t) = -\rho_u c_b \left(1 - \frac{T_u}{T_b}\right) S_L.$$

If it is assumed that the fluid expansion velocity is the same before and after time of impact one can use eq. (4.8):

$$u_b = S_L \left(\frac{\rho_u}{\rho_b} - 1\right),$$

to rewrite eq. (4.9) into:

$$\Delta P_{\min} = \rho u_p u_b = \rho u_p S_L \left(\frac{\rho_u}{\rho_b} - 1\right). \tag{4.17}$$

If it then is assumed that the density, ρ, can be linearized by the burned gas density, ρ_b, and the terms are moved around a bit the equations yield:

$$\Delta P_{\min} = \rho_u u_p \left(1 - \frac{\rho_b}{\rho_u}\right) S_L. \tag{4.18}$$

If one can then show that $\rho_b/\rho_u = T_u/T_b$ and $u_p = c_b$ then eqs. (4.9) and (4.14) are equivalent (in absolute values). This claim was investigated in the project work of fall 2012. It was shown that there was indeed a close link between the two. In the project work it was also shown that the propagation speed of the pressure wave was approximetaly the same as the sonic velocity ($u_p = C_s$). The claim that these formulas are equivalent will also be investigated to a degree in section 6.1.2.

In Talei et al. [37] there are some remarks regarding their numerical results which is important to note. In the far field in the planar case the pressure has a very similar temporal history to that of the origin, this is however not the case for the axisymmetric and spherically symmetric cases. For both of these cases the peak pressure in the far field is small compared to the near field. This is not surprising as classical acoustics dictates a scaling of $\frac{1}{\sqrt{r}}$ in the axisymmetric case and $\frac{1}{R}$ in the spherically symmetric case. It is also noted that the pressure fall is largest in the planar case and smallest in the spherically symmetric case (see fig. 4.2).

5 The Numerical Method

In this chapter the numerical method used in the simulations will be presented. Simulations of two dimensional laminar imploding circular flame fronts have been the main focus of the thesis. One dimensional simulations of laminar opposing flame fronts have also been performed to establish modeling conditions for the two dimensional simulations, evaluate the boundary influence on the simulations, and provide comparable simulation results. In addition a pre-study for three dimensional simulation of an inwards burning sphere of fuel has been done. The candidate did simulations in one dimension in the project work of fall 2012. Some results from this study will be repeated. The generation of acoustic waves is the focal point of the studies.

The domains used in the simulations are visualized in fig. 5.1.

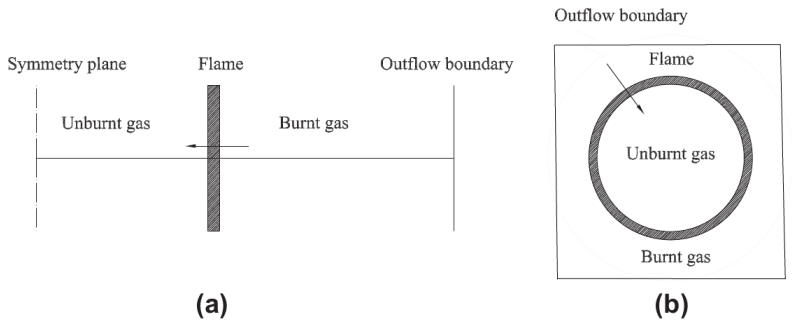

Figure 5.1: Schematic of computational domain for a) planar, b) axisymmetric and spherically symmetric flame annihiliation (not to scale) (From Talei et al. [38]). Outflow boundary in b) is changed from circular to square.)

As Talei et al. [37] notes, DNS of sound generated by a premixed flame is a challenge. Several points of notice include adequate resolution of the flame, ensuring a large enough domain to resolve the larger long-wavelengths of the radiated sound, and avoid spurious effects at the boundaries.

5.1 The DNS Code

The S3D code is a parallel DNS code developed at the Combustion Research Facility at Sandia National Laboratories (Hawkes et al. [18]). S3D is written in

FORTRAN 90 and the algorithm implemented solves the compressible Navier-Stokes equations in conservative form on a structured cartesian mesh. An eight order explicit centered finite difference scheme is used for the spatial derivatives, while a fourth order six-stage explicit Runge-Kutta integration method is implemented as the time integrator.

Several studies have been done using the S3D code. Hawkes and Chen [17] tested the code for premixed combustion, and there has also been done tests with non-premixed flames and auto-ignition. Gruber [14] implemented fluid wall boundary conditions into the S3D code and used it for research on laminar and turbulent v-flames in channels (Gruber et al. [13]). Chen et al. [6] used the S3D code in a terascale DNS of turbulent combustion.

As the S3D code solves the full compressible Navier-Stokes, total energy, species and mass continuity equations coupled with detailed chemistry, it is a massive computational undertaking to process. The governing equations are also supplemented by additional constitutive relationships, as the ideal gas equation of state, models for reaction rates, molecular transport and thermodynamic properties.

5.1.1 The Conservation Equations

The notation and equations are from Chen et al. [6], where a terascale DNS of turbulent combustion is performed using S3D. These equations are chosen as they show all the fluid dynamics and chemical reactions solved by the S3D code, and is ment for illustrative purposes in this thesis.

The governing equations for reacting flows in conservative form can be written as:

$$\frac{\partial \rho}{\partial t} = -\nabla_\beta \cdot (\rho \vec{u}_\beta), \tag{5.1}$$

$$\frac{\partial (\rho \vec{u}_\alpha)}{\partial t} = -\nabla_\beta \cdot (\rho \vec{u}_\alpha \vec{u}_\beta) + \nabla_\beta \cdot \underline{\tau}_{\beta\alpha} - \nabla_\alpha P + \sum_{i=1}^{N_s} Y_i \vec{f}_{\alpha i}, \tag{5.2}$$

$$\begin{aligned} \frac{\partial (\rho e_0)}{\partial t} =& -\nabla_\beta \cdot [\vec{u}_\beta (\rho e_0 + p)] + \nabla_\beta \cdot \left(\underline{\tau}_{\beta\alpha} \cdot \vec{u}_\alpha\right) \\ & - \nabla_\beta \cdot \vec{q}_\beta + \rho \sum_{i=1}^{N_s} Y_i \vec{f}_{\alpha i} \cdot \left(\vec{V}_{\alpha i} + \vec{u}_\alpha\right), \end{aligned} \tag{5.3}$$

$$\frac{\partial (\rho Y_i)}{\partial t} = -\nabla_\beta \cdot (\rho Y_i \vec{u}_\beta) - \nabla_\beta \cdot \left(\rho Y_i \vec{V}_{\beta i}\right) + W_i \dot{\omega}_i, \tag{5.4}$$

where ∇_β is the gradient operator in direction β, Y_i is the mass fraction of species i, W_i is the molecular weight of species i, $\underline{\tau}_{\beta\alpha}$ is the stress tensor, $\vec{f}_{\alpha i}$ is the body force on species i in direction α, $\vec{q}_\beta$ is the heat flux vector, $\vec{V}_{\beta i}$ is the species mass diffusion velocity, $\dot{\omega}_i$ is the molar production rate of species i and e_0 is the specific total energy (internal plus kinetic energy).

To close the system of equations one also need thermodynamic relations (to express coupling between pressure and the mixture compositions, and to express the species enthalpies), an expression for the stress tensor, the heat flux, the diffusion velocities and the chemical source term. Together these constitute a closed system of equations, which can be solved numerically (Hilbert et al. [20]). For a complete overview of the equations in the closed system, the reader is referred to Chen et al. [6].

5.2 One Dimensional Simulations

In the candidate's project work done in the fall of 2012, one dimensional simulations were done for both detailed and simple chemistry representation. In this thesis the focus is on the study of sound generation for detailed chemistry representation problems and consequently only the results from this representation will be used for comparison.

The one dimensional simulations serve two purposes in this master thesis. One, the results obtained will be compared with the results obtained from the two dimensional simulations, and two, the two dimensional simulations will be restricted by them. The first of these two purposes is self-explaining, while the second will be explained in short order.

Table 5.1: Case parameters from one dimensional simulations.

ϕ	P (atm)	Grid points, N_x	Domain, L_x (m)	Timestep, t_{step} (s)
0.3	1	1920	0.01	1×10^{-9}
0.5	1	1920	0.01	1×10^{-9}
0.8	1	1920	0.01	1×10^{-9}
1.5	1	1920	0.01	1×10^{-9}

In table 5.1 the parameters used in the project work for a given set of

simulations are given (all simulations at $P = 1\,\text{atm}$). In the two dimensional simulations the resolution is too high to be of practical use. That is, the simulation time will be very high when using 1920 grid points in two directions. The simulation time will be from approximately 20 days with 144 cores, up to the triple of that (this is based on some preliminary two dimensional simulations and the simulation details given in section 5.3). The number of grid points is therefore reduced as much as possible, without loosing the resolution of or changing the solution.

This was done by performing the one dimensional simulations once more with a lower number of grid points. The same set-up as in the project work (and for the two dimensional simulations in this thesis) was used. It was found that for the cases listed in table 5.2 the resolution could be divided by four, while the timestep should be held at the same level.

Table 5.2: Updated case parameters from one dimensional simulations.

ϕ	P (atm)	Grid points, N_x	Domain, L_x (m)	Timestep, t_{step} (s)
0.3	1	480	0.01	1×10^{-9}
0.5	1	480	0.01	1×10^{-9}
0.8	1	480	0.01	1×10^{-9}
1.5	1	480	0.01	1×10^{-9}

In the project work there was also done simulations at pressure levels of 5 atm and 10 atm for all levels of fuel equivalence ratio. These cases were also investigated in a similar manner as the ones above, but it was found that one could not decrease the number of grid points sufficiently and the simulations would consequently not be possible to undertake in the given time frame of this thesis. They were therefore not devoted more time.

5.3 Two Dimensional Simulations

In the two dimensional simulations the main goals were:

- Modification and validation of DNS code for two dimensional imploding flame fronts. This involves adaptation of consistantly similar boundary conditions.

- Identification of modeling conditions for two dimensional simulations.
- Carry out simulations on for two dimensional imploding flame fronts.
- Analysis of results and identification of driving parameters for instabilities.

In the two dimensional simulations non-reflecting boundary conditions were used for the western, eastern, southern and northern boundaries and detailed chemistry representation has been used to represent the combustion as accurate as possible. The flow is set to laminar conditions. In two dimensional simulations the turbulence would have to be modeled, as turbulence is a three dimensional phenomena. In this thesis laminar conditions is chosen as the first and foremost goal is to make the code simulate the two dimensional case without any errors. Under laminar conditions this is easier to verify, and the flow will be simpler than a turbulent flow (no turbulent scales involved). The initial velocity field is set to zero in the whole domain. This is known to be wrong, as the expected result is an outflow from the domain (higher temperature in the burned domain leads to lower density). The possibility to correct the initial velocity field is held as an option if the solution does not converge. The initial value for flame thickness is set according to the fact that it decreases with increasing equivalence ratio and pressure (see section 2.2.1). This leads to the realization that thinner flames needs a higher resolution to be fully captured (all details of the flame characteristics captured). Care has been taken to ensure a proper resolution over the flame, and a criterion of minimum ten points over the flame has been used.

Table 5.3: Case parameters for two dimensional simulations.

ϕ	P (atm)	Grid points, N_x	Grid points, N_y	Domain, L_x (m)	Domain, L_y (m)	Timestep, t_{step} (s)
0.3	1	480	480	0.01	0.01	1×10^{-9}
0.5	1	480	480	0.01	0.01	1×10^{-9}
0.8	1	480	480	0.01	0.01	1×10^{-9}
1.5	1	480	480	0.01	0.01	1×10^{-9}

In table 5.3 the case parameters for the two dimensional case are presented. As a simulation in two dimensions is a lot more costly than a one dimensional simulation, a smaller pre-study to investigate the resolution needed was performed in one dimension (see section 5.2). This leads to a realization that for $P = 1\,\text{atm}$

the number of grid points compared to the corresponding one dimensional case can be divided by four in each dimension. This will have a significant impact on the simulation time as the number of grid points is reduced by a factor of sixteen compared to a two dimensional case using the same parameters as the corresponding one dimensional case from table 5.1.

The domain and initial flame set-up is supposed to model the pinch-off of a unburned gas bubble. In fig. 3.2 both this process and the process of an imploding gas bubble is shown. As the fresh gas "push" on the flame front a pocket of unburned gas is formed. This pocket will then be pinched off, creating an acoustic wave propagating from the pinch-off area. In Brear et al. [5] the dilatation field at both pinch-off and annihilation is visualized (see fig. 5.2).

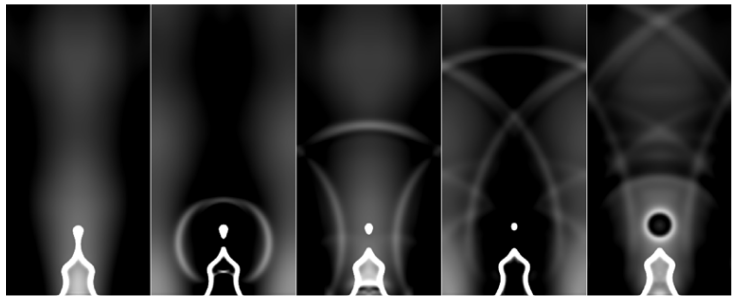

Figure 5.2: Instantaneous dilatation field during the forcing period (Brear et al. [5]).

The same definition of time of impact as the one in section 4 is used. τ_i then denotes the instant when the temperature in the middle of the domain, $T(x_{\text{center}})$, changes from the initial temperature in the unburned domain.

In the two dimensional simulations the expected result is pressure waves moving out of the domain after τ_i at the speed of sound. These pressure waves are expected to have a smaller amplitude than in the one dimensional simulations (see section 4.3). An example is when one throws a stone in a pond. There is not one single wave, but several waves moving outwards from where the stone hit the water. This is explained through overshoot (overcompensation). In the one dimensional simulations only one pressure wave was observed, and this may also be the case in the two dimensional simulations. This is then expected to be a domain issue. As the domain has a limited length, the pressure wave will move outwards, and before the pressure rise can occur and another pressure wave is formed, the boundary conditions break down (that is, there is an inflow at the

boundary).

The results will be investigated along one line (say $y = 0.5$) in the domain, and one would then expect a similar profile (for example for the temperature profile) as for the one dimensional simulations (given the same conditions) for the same parameter in most cases (those which are not influenced by the domain scaling effects). The diffusion effects are predicted to have a larger impact in two dimensions as the flame front circumference will be reduced gradually as the flame burns inwards (scaling).

There are several interesting factors to look at when comparing the numerical results from the one and two dimensional simulations. In this report the focus will be on the characteristics of the flame, i.e. the flame propagation speed, the pressure drop at impact, etc.. The following parameters were measured from the simulations with detailed chemistry representation using Tec360 [2]:

- The fluid expansion velocity - u_b.
- The flame thickness - δ_f.
- The density in the burned domain - ρ_b.
- The density in the unburned domain - ρ_u.
- The laminar flame propagation velocity - S_L.
- The propagation speed of the pressure wave - u_p.
- The pressure difference between the burned and unburned domain before time of impact - ΔP.
- The pressure drop at impact - $\Delta P_{\min}$.

The parameters were measured in the following way:

- u_b, ρ_b and ρ_u are measured directly. These have their individual plots in Tec360 where the values can be read. It is important to choose a timestep where one is certain of the validity of the value. That is, well before annihilation and well after the initialization process.
- δ_f is found from the reaction rate of H_2. It is assumed that the reaction rate width of H_2 is approximetaly the same as the flame width.

- S_L is found from the simple relation $S_L = \frac{\Delta x}{\Delta t}$, where Δx and Δt are found from a plot of ρ at two different time steps. Δx is then the distance between the two plots in the transition area from the unburned to burned domain, and Δt is the time interval between the two plots.
- u_p is measured from a plot of the pressure at two times after τ_i (that is, when the pressure is decreasing and a pressure front is observed). The relation $u_p = \frac{\Delta x}{\Delta t}$, where the values are obtained in the linear region of the pressure wave (as linear as possible). Δx is the distance between the pressure lines at a fixed pressure in the linear region of the pressure wave and Δt is the time between the plots.
- ΔP is measured before τ_i (such that the flames can not feel each other). It is defined as $\Delta P = P_u - P_b$, where P_u and P_b is the pressure in the unburned and burned domain, respectively.
- $\Delta P_{\min}$ is defined as $\Delta P_{\min} = P_{\text{init}} - P_{\min}$, where P_{init} is the initial set pressure in the simulations and $P_{\min}$ is the minimum pressure (at x_{centre}).

It is worth mentioning that the measuring process is approximetaly the same for both one and two dimensional simulations.

5.3.1 The procedure

The first objective was to get the code running the specified case, namely a square domain with a circular (axisymmetric) flame placed on it. Both the input files and source files in the S3D code had to be manipulated to get the desired case. In this section the simplest case ($\phi = 1.5$ and $P = 1\,\text{atm}$) has been used as the testcase throughout.

Add circular flame

First the case of a circular flame was added to the source code and to the input files in the S3D code. The case was implemented such that the shape of the flame (circular) was locked, but the positioning and radius of the flame could be set in the input files. The initialization of the flame also made it necessary to modify the function which define the temperature transition from burned to unburned (which basically means the flame shape). The old function use a vector input, but as the flame was implemented using polar coordinates a point-by-point approach had to be used (see appendix D).

The first testcases was then simulated using the initialized flame on the domain, and with a velocity field set to zero. The radius of the flame was set to

0.4 cm. As mentioned for the one dimensional cases, this velocity field is obviously wrong, but if the solution stabilizes the initial value of the velocity field is of no interest. However, the first testcase showed a problem at the boundaries. The boundaries were set to only handle outflow (as this is the only physical flow that can occur) from the domain. After some simulation time, there was an inflow at several points (near the corner of the north-west boundary) in the domain. This caused the simulations to break down (the total error exploded from approximately 10^{-7} to 10^{3}). In addition the flame was moving southwest in the domain. This was caused by an induced velocity in the unburned area in the southwestern direction (the velocity in the unburned area should be zero).

Add initial velocity field
The initial velocity field was then manipulated to simulate the expected outflow solution. This approach's intention was to diminish the initial error and thereby try to obtain a stable solution. To do this the velocity field was modeled as a graded outflow. This implies that at the boundary the expected fluid expansion velocity for the given case parameters in the unburned domain was used (this value was chosen from the results of the one dimensional simulations). The function to define the flame shape was used to define the grading of the velocity field as well. This, together with simple algebraic relations to ensure the same mass flow in all directions, gave the initial velocity field as shown in fig. 5.3 (see appendix E for code implementation). Unfortunately this was not enough to get a stable solution. The simulations broke down some time before annihilation.

Reduce radius of the circular flame
The next approach to the simulation problems was to reduce the radius of the circular flame (the initial velocity field was set back to zero). This was tried to reduce the influence of the boundaries on the simulation. A too strong coupling with the boundaries can distort the simulation results, and make the initial field of the physical parameters unsteady and unphysical. The radiuses tried were as following: 0.3 cm, 0.25 cm and 0.2 cm. This was shown to have no effect, as the simulations would without exception break down some time before annihilation.

Searching in the source files
As the simulations using the original source code modified with the circular flame did not yield the desired results, and a boundary issue seemed to be the problem, two source code files were investigated thoroughly in search of programming errors. The two files were nscbc.f90 and update_L.f90. nscbc.f90

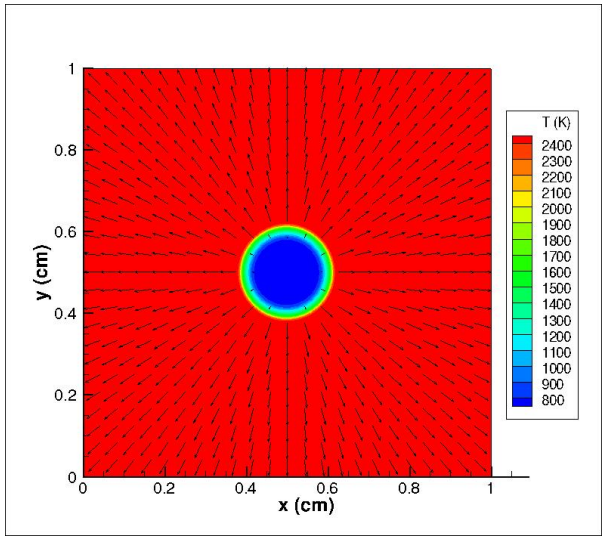

Figure 5.3: Initial velocity and temperature field on a two dimensional domain.

imposes Navier-Stokes Characteristic boundary conditions at all open boundaries in the boundary-normal direction. This is done by method of characteristics to eliminate waves in each primitive variable as they propagate through a boundary. In update_L.f90 boundary conditions is imposed for open boundaries by setting characteristic wave amplitudes.

An error at the northern boundary was found and corrected in nscbc.f90. This error updated a factor in the boundary flow incorrectly. Unfortunately this did not do much for the overall stability of the simulations.

In update_L.f90 it was found that the western and eastern, and southern and northern boundaries were not solved in the same way. There are, as it often is in programming, a number of ways to get the same problem solved. It is important that the same method is used on all boundaries to ensure symmetry/similarity. The two methods used are referred to as “simple” and “refined”. The difference between the simple and refined code (in update_L.f90) is the method used to calculate the characteristic wave amplitudes. The refined code has more terms in the code to calculate the flow characteristics, while the simple code uses an approach with fewer terms. The code in update_L.f90 was therefore changed so that all boundaries were alike. This was done in four different ways:

- The simplest code was used on all boundaries without a damping term.
- The simplest code was used on all boundaries with a damping term.
- The refined code was used on all boundaries without a damping term.
- The refined code was used on all boundaries with a damping term.

The damping term can be seen as a spring which brings the boundary values back to a prescribed value. In this case it is used to ensure outflow on the boundaries. These approaches did not, however, bear fruits. The velocity field during the simulations (before annihilation) was not equal to zero in the unburned domain in any of the cases. It must be emphasized that the alterations done in update_L.f90 was based on the already implemented code (i.e. the western boundary code was used as a guide for the eastern).

Increase number of grid points
It was also attempted to increase the number of grid points in the domain. This was done mainly to investigate if two dimensional effects demanded a higher resolution to be fully described. The domain was modeled with four times the original grid points in both x- and y-direction (1920 grid points) which gives a total number of grid points sixteen times that of the original case. This naturally implies that a lot more computational force was needed. The motivation for increasing the number of grid points did not relate to the resolution of the flame itself (which was identified earlier as an important point when numerically investigating combustion flames), but to enhance the resolution of the initialization of the circular flame. It was suspected that the circle was to "edgy" to give the right characteristics. It was however shown that an increase in the number of grid points did not alter the solution.

New source code
As none of the above approaches gave any reasonable results, new versions of update_L.f90 were acquired.

Through Damir Valiev (CEFRC postdoc at Princeton University/Sandia National Laboratories) two versions of update_L.f90 were acquired: An update_L.f90 by Chunsang Yoo and an update_L.f90 which Valiev had modified. Both codes were tested on two dimensional simulations in the xy-plane, but did not yield the desired results. In fig. 5.4 the pressure fields are depicted right after annihilation (together with iso-lines for the temperature and the velocity field represented by the velocity vectors). The figures clearly shows the non-symmetry

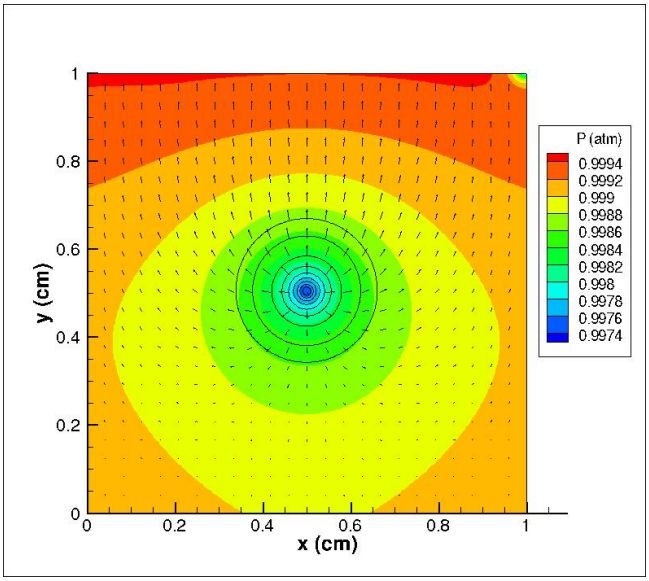

(a) Chunsang Yoo's update_L.f90.

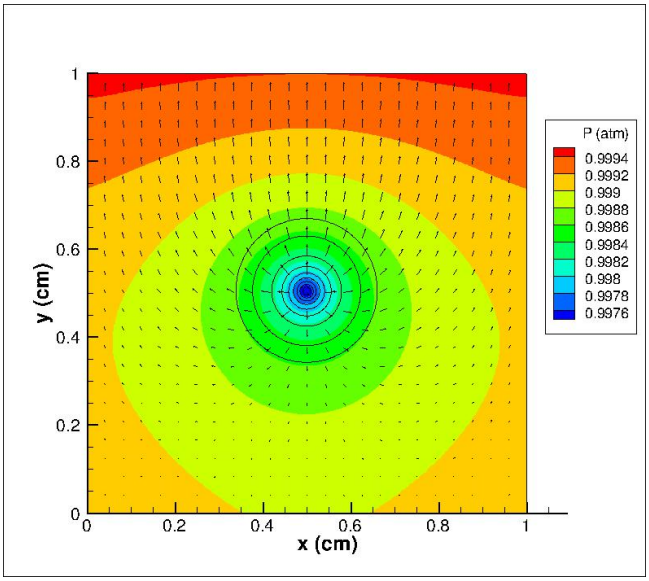

(b) Damir Valiev's modified update_L.f90.

Figure 5.4: Pressure field, velocity vectors and iso-temperature lines on a two dimensional domain 1.

of the simulations. It was noted that the velocity field seems to be drawn towards the northern boundary. Therefore a closer look was taken at this boundary. In fig. 5.5 the temperature field just after annihilation (Valievs code) together with the pressure (the colors) is shown. Here it is clear that the temperature and pressure on the northern boundary is higher than the other boundaries. It was found that this temperature difference between the boundary is not present in the initial field, but grows rapidly early in the simulations and then settles at a steady level. This is also seen in the velocity field, as it seems to settle on a steady state where the velocity in the northern half of the domain is larger. It is

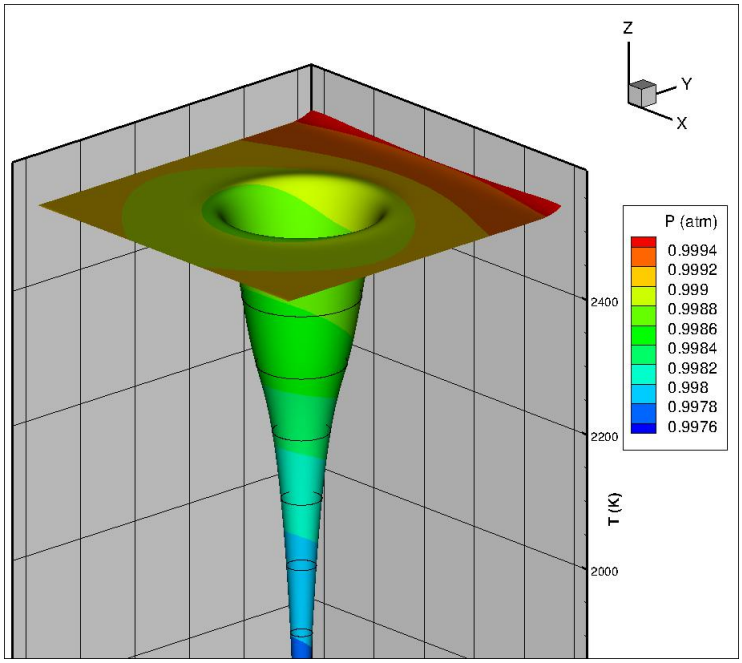

Figure 5.5: Temperature field in a two dimensioal simulation just after annihilation using Damir Valiev's modified update_L.f90.

important to note that the parameters are linked. The pressure, density, velocity field and so forth are thus all wrong, and the likely cause is a problem at the northern boundary (y=L). Therefore a search was conducted in the source code to try to find the culprit. This search did yield some results as it was found that the density was set to zero at some point in the simulations. This did alter the

solution, but a fix to this problem was not pursued as other ways to work around the problem was prioritized (to correct the source code seemed to be a massive undertaking, with no guarantees when it came to the final result).

Hemanth Kolla (at Sandia National Laboratories) provided a different update_L.f90 which was symmetrical in the yz-plane. This then involved some further alterations to the source code, as the two dimensional case had to be implemented in the yz-plane (init_flame.90 and flame.in had to be altered). When these alterations were done the new source code was tested on two dimensional simulations in the yz-plane. The code however was not stable and only did the initialization of the flame. Several different approaches were taken to try to fix the problem:

- Alter Hemanth's update_L.f90 to work in xy-plane.
- Modify a version of update_L.f90 by combining Chunsang Yoo's original version and Hemanth's version.
- Finding the error in Hemanth's version of update_L.f90.

After altering Hemanth's code to work in the xy-plane (which was done by using the y- and z-directions in update_L.f90 as guides for the x-direction), the code was tested in a two dimensional simulation. The results was yet again not symmetrical. In fig. 5.6a the pressure and velocity field is shown and it is clear that there is an outflow problem at the eastern boundary. Further investigation also reveals that the same problem as in Valiev and Chunsang Yoo's update_L.f90 at the northern boundary is still present. The obvious reasons for the errors in this simulation are programming errors done by the writer of this paper. It is obvious that the western and eastern boundary is not symmetrical, something which is a "new" error. However, the "old" error is also contained in this simulation.

In the combined version Chunsang Yoo's version of update_L.f90 was manipulated using Hemanth's version (symmetrical in the yz-plane). The intended effect was to get a symmetrical result by using the "good sides" of both versions. As seen in fig. 5.6b this did however not work out the way intended. The pressure and velocity field are clearly way of the desired and it is noted that during the simulation several unintended effects was observed. Among these were a sudden pressure wave coming in from the southern border. It is also noted that the problem at the northern boundary is still an issue.

In the two approaches above the simulations in two dimensions were done in the xy-plane with the normal settings as given earlier (see table 5.3, $\phi = 1.5$).

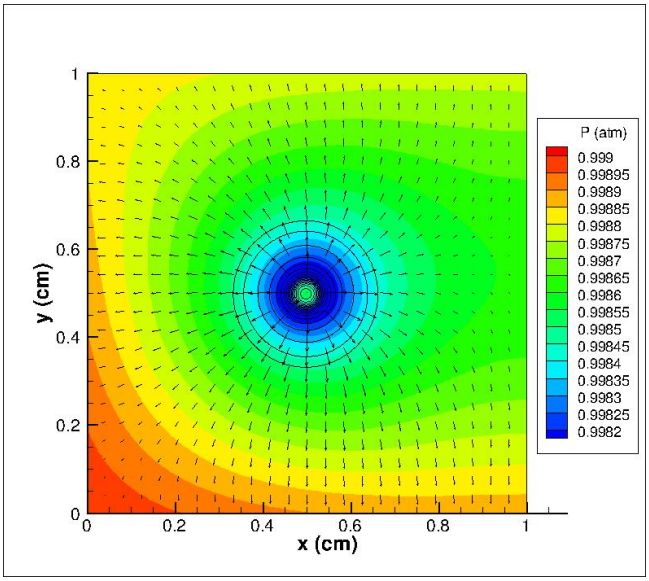

(a) Hemanth's update_L.f90.

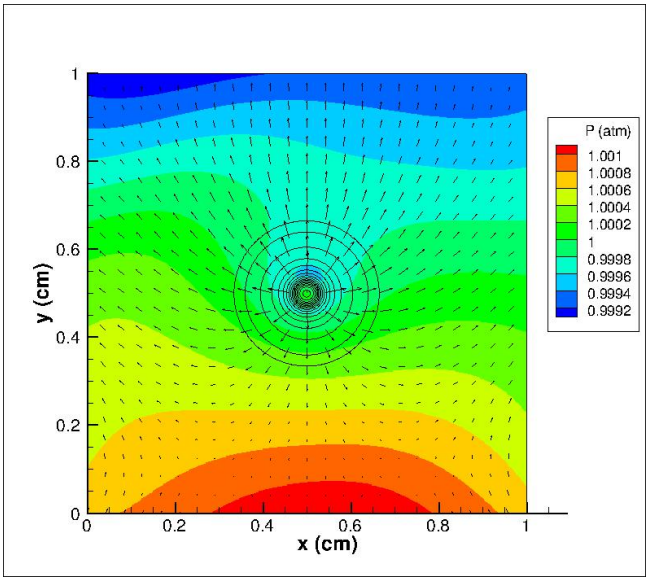

(b) The combined update_L.f90.

Figure 5.6: Pressure field, velocity vectors and iso-temperature lines on a two dimensional domain 2.

The last approach was more of a treasure hunt. The search mainly consisted of going into the source code, identifying possible locations for the error by writing simple statements, and repeating this procedure until the error was found. This search for the error eventually led to a term in update_L.f90, namely S_p. This is a source term for the pressure and is mainly important for boundary flow problems (that is, when interactions/reactions take place at the boundary). The error consisted in a division by zero, such that the simulations involved NaNs (Not a Number), which in turn broke down the simulations. It was agreed upon to try to set this term to zero as no reactions are supposed to take place at the boundaries. It was found that the simulations now ran smoothly and seemed symmetrical, and that the annihilation event was simulated as planned. However, it is important to be sure that this does not alter the solution (gives unphysical effects), and one of the parameters which is especially important is the radius of the initial flame. If the flame is too large (large diameter) it will be to close to the boundaries and hence be a boundary problem and S_p will potentially have a large impact on the solution. If the flame is too small (small diameter) the flame will not be able to reach a steady state (steady burning velocity, no pressure fluctuations from intial state) before the reaction takes place, which will then lead to unreliable results. Simulations were therefore attempted with several different radiuses, and it was found that a radius of 2 mm was a good choice for the given cases in table 5.3.

Running the simulations

The input files in the S3D code were changed according to the numerical parameters presented in table 5.3.

The flame was initialized such that there was minimal interaction with the boundaries, and minimal interaction between the flame (smaller radius equals more interaction). In the simulations performed the flame was placed at a radius of 2 mm, in a domain of 10 mm. Care had to be taken to ensure proper resolution, and the actual annihilation of the flame (the number of timesteps simulated differs from case to case).

The S3D code produce one resultfile per processor per timestep. The files produced by the code were post-processed to create plt-files as these files are more efficiently read by Tec360. These plt-files were then processed in Tec360 and the measurements were performed as specified in section 5.3.

5.4 Three Dimensional Simulations

In the three dimensional simulations the main goals were:

- Initialize a spherical flame in a cubic domain.
- Identify modeling conditions for 3D simulations.

In the three dimensional simulations non-reflecting boundary conditions were used at all the boundaries. The domain was cubical with a spherical flame initialized within. Detailed chemistry representation has been used to represent the combustion at the most accurate level possible. The flow condition was set to laminar and the initial velocity field was set to zero, which is known to be wrong (see explanation in section 5.3). The initial value for the flame thickness was set as for the one dimensional and two dimensional simulations. A criterion of a minimum of ten points over the flame has been used to ensure proper resolution of the flame.

In table 5.4 the case parameters for the three dimensional simulations/initialization are presented. In three dimensions the simulations are a lot more costly than in one or two dimension. The study therefore relies on the pre-study done in section 5.2 to minimize the number of grid points needed to ensure proper resolution of the flame and give reasonable simulation times.

Table 5.4: Case parameters for three dimensional simulations.

ϕ	P (atm)	Grid points, N_x	Grid points, N_y	Grid points, N_z	Domain, L_x (m)	Domain, L_y (m)	Domain, L_z (m)	Timestep, t_{step} (s)
1.5	1	480	480	480	0.01	0.01	0.01	1×10^{-9}

The spherical flame is supposed to model the actual annihilation of a inwards burning gas bubble. In fig. 5.2 the pinch-off process and the annihilation of the gas bubble is shown. The annihilation then creates an acoustic wave propagating from the annihilation area.

The expected result is pressure waves moving out of the domain at τ_i at the speed of sound. The diffusion effects are predicted to have a larger impact in three dimensions as the flame front circumference (radius of the sphere) will be reduced gradually as the flame burns inwards. It is also expected (based on Talei et al. [37]) that the pressure drop after τ_i will be smaller than in the planar and axisymmetric respective cases.

5.4.1 The procedure

The main objective was to get a correct initialization of the spherical flame. To do this the source code had to be altered to accomodate a spherical three dimensional flame. These changes were mostly done in initialize_flame.f90 (see appendices D and E) while small alterations to the input files was also necessary (such as setting up the flame characteristics in flame.in).

To summarize: The case of a spherical flame was added to the source code and to the input files. The case was implemented such that the position and radius of the flame could be set in the input files. The same function as was used in (and developed for) the two dimensional simulations to define the temperature transition was used here.

Several testcases using the simplest scheme ($\phi = 1.5$ at $P = 1\,\text{atm}$) were simulated. Due to a small programming error the y-plane was copied over in the z-plane, and thereby erasing some of the correctly initialized sphere and instead initializing a cylindrical flame. This error was corrected and the initialization process now showed no problems. (See fig. 6.2 for a visualization of the temperature field of the initialized inwards burning sphere.)

It was attempted to simulate beyond initialization, but the same problems as in two dimensions quickly emerged. The simulation, after all the alterations mentioned in section 5.3.1 were done, was not symmetric as the code was only symmetric in two directions (y- and z-direction). It was attempted to alter the source code to be symmetric in all three directions, but as for the two dimensional case, a solution was not found (only two directions symmetric).

It was also found that in the given time frame a three dimensional simulation would not be possible due to long simulation times.

It is expected that the pre-study done in one dimension will also hold for three dimension. That is, the simulation parameters given in table 5.4 should contain the solution in an adequate fashion, while keeping the simulation time at a minimum.

6 Results and Discussion

In this chapter the results of the numerical simulations will be presented and discussed. The results will be compared with the one dimensional simulations done in the candidate's project work in fall 2012, as well as with the literature. The results will be thoroughly discussed to give light to any deviations.

The results will be presented in the following order:

- Two Dimensional Simulations:
  - Measured parameters from Two Dimensional Simulations.
  - Comparison of analytical and numerical results.
  - Comparison of measured parameters from One and Two Dimensional Simulations.
- Three Dimensional Simulations.

6.1 Two Dimensional Simulations

The results for the two dimensional simulations will be split into three parts. First the parameters listed in section 5.3 and their measured values are presented in tabular form. Then the analytical expressions from section 4 are calculated using the numerical results from the simulations. In the last section the results from the one and two dimensional simulations are compared.

6.1.1 Measured parameters from Two Dimensional Simulations

In tables 6.1 and 6.2 the measured results in the various simulations are listed. It is noted that the values should be used carefully, as they are manually read from plots with a certain resolution. It is noted that for $\phi = 0.3$ the propagation speed of the pressure wave and the pressure drop after τ_i are not given. This is due to problems with measuring them accurately (due to small amplitudes and resolution of the result files).

Expected results and measuring

Based on the expected results (see section 5.3), the actual results raised some suspicions. Specifically the values of u_b, u_p and $\Delta P_{\min}$.

To try to address these suspicions some smaller scale studies were conducted. One of the main things to address was possible boundary influence on the simulation solutions. The question asked was as follows: "Did the boundaries

Table 6.1: Measured parameters 1.

ϕ	u_b (m/s)	δ_f (10^{-4} m)	ρ_b (kg/m^3)	ρ_u (kg/m^3)	S_L (m/s)
0.3	1.63	4.256	0.208 34	0.421 09	3.136
0.5	5.78	2.573	0.160 61	0.394 30	6.349
0.8	10.00	2.342	0.127 52	0.360 32	9.506
1.5	14.24	1.960	0.104 26	0.300 90	12.914

Table 6.2: Measured parameters 2.

ϕ	C_s (m/s)	u_p (m/s)	ΔP (Pa)	$\Delta P_{\min}$ (Pa)	T_b (K)
0.3	788.6	-	2.03	-	1598.80
0.5	897.0	35.2	13.19	28.8	1994.59
0.8	1010.8	39.0	30.43	145.3	2367.59
1.5	1120.5	172.7	45.95	297.9	2435.71

have an influence on the solution in the two dimensional simulations, and is the boundary influence coupled with update_L.f90?" A case in one dimension in the y-direction was simulated to check the influence of update_L.f90 (the x-direction cases are from the project work of fall 2012 and were done with the old update_L.f90), using the same set-up as in the project work ($\phi = 1.5$, $P = 1\,\text{atm}$). The corresponding x- and y-direction cases were then compared. The results indicated that with the new update_L.f90 there was a longer initialization period. In both cases the pressure increases at initialization, and then gradually decreases to the initial pressure (here $P = 1\,\text{atm}$). The pressure did not manage to reach the initial pressure before τ_i in the simulated y-direction case. This influences the pressure drop after τ_i (it becomes smaller). This realization means that the same would probably be true for the two dimensional cases. This implies that several test cases have to be simulated. The boundary influence of all the cases in table 5.3 have to be investigated. To make a first estimate of the boundary influence, one dimensional simulations of the corresponding cases should be done with longer domains. These should then be compared with the results from the 1 cm domain. Then the full two dimensional simulations should be done using larger domains.

As there was no time to fully address this complication, some initial simu-

lations were done to give a headstart for further investigation. A case in one dimension with a longer domain ($\phi = 1.5$, $P = 1\,\text{atm}$, $L_y = 5\,\text{cm}$) was simulated to test the theory. The results showed that the pressure at τ_i was approximetaly 1 atm in the center of the domain, and that the pressure fall after τ_i corresponded with a similar case using the old update_L.f90. This indicates that in this specific case the boundary had an influence on the results which can not be tolerated. A case in two dimensions was also investigated. Due to problems with available computing power, high computing demands and long computing time, the simplest case ($\phi = 1.5$, $P = 1\,\text{atm}$) was simulated (shortest simulation time). The domain length in both dimensions was set to 3 cm, with the same resolution per cm as in table 5.3. The flame was positioned at a radius of 1 cm from the center of the domain. The goal was to have as little influence from the boundaries, and as little interaction due to two dimensional effects (circumference effects), as possible. The simulation revealed some interesting results. The value of u_b indicated that the value of u_b in table 6.1 is under-measured. More simulations are needed to verify this claim. The pressure drop after τ_i was not possible to measure due to some simulation issues. More simulations needs to be done to clarify the relation of boundary influence with the pressure drop after τ_i. The simulations requested have to be done under the same conditions ($P = 1\,\text{atm}$) at all fuel equivalence levels, but the resolution, grid length, and so forth have to be changed according to the issue under the scope.

The values of u_b was difficult to measure, as the values did not stabilize at a given level (as they did in the one dimensional simulations). This is related to the increasing circumference as the mass flow moves outwards towards the boundaries of the domain. This will lead to a decrease in u_b as the flow moves outwards (and the circumference increases). It was also noted that the maximum value of u_b decreased with decreasing radius. Nils E. Haugen[3] noted that the fluid expansion velocity in the two dimensional simulations, $u_{b,2\text{D}}$ should have the following relation to the one dimensional fluid expansion velocity, $u_{b,1\text{D}}$:

$$u_{b,2\text{D}} = u_{b,1\text{D}} \frac{r_{\text{flame}}}{r_{\text{measured}}}, \tag{6.1}$$

where r_{measured} is the radius where one measures the fluid expansion velocity in the two dimensional case, and r_{flame} is the distance from the center of the domain to the flame front. This also implies that, as the flame front (r_{flame}) change its relative position to r_{measured}, the measurement of u_b should be done as early as possible after initialization. u_b was therefore measured as the maximum

[3]Personal communication.

velocity behind the flame as early as possible after the initialization process. This is in agreement with the remarks done in section 4.3 regarding the axisymmetric cases. The simulation in two dimensions described in the previous paragraph indicates that u_b is under-measured, which is in agreement with eq. (6.1). To be confirmed this calls for further investigation. In fig. 6.1 the v-component of the velocity field is presented. The lines represent values at different z-values, where the maximum amplitude line is the line representing $z = 0.5\,\text{cm}$, which is where the w-component of the velocity will be approximetaly zero.

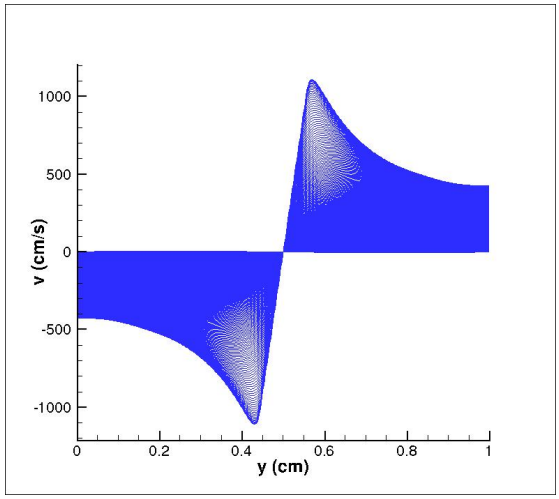

Figure 6.1: The v-component of the velocity field at an instant after initialization.

Note that in table 6.2 the speed of sound, C_s, in column two is not measured, but rather obtained using Gaseq [28] (a freely available computational code), is used as a reference of the speed of sound under the given conditions.

The measurements of u_p was a challenge. It was expected that the propagation speed of the pressure wave would be approximetaly equal to the reference speed of sound. This is clearly not the case from the given results. These values were obtained using the method described in section 5.3. The validity and accuracy of this method in the two dimensional simulation are therefore under question. It was noted that the value of u_p using the method described was dependent on the domain. The propagation speed of the pressure wave "increased" with increasing radius. Therefore u_p was measured in two other ways:

- From a one dimensional plot of the pressure at two instants after τ_i. The relation $u_p = \frac{\Delta x}{\Delta t}$ is used, where Δx is the horizontal component of the minimum distance between the pressure lines.
- From a two dimensional plot of the contour lines of the pressure at two instants after τ_i. The relation $u_p = \frac{\Delta x}{\Delta t}$ is used, where Δx is the distance between the contour lines.

The first method gave results of smaller deviation by domain, and with a slightly larger u_p (about 11% of the reference speed of sound). The second method gave approximetaly the same results as the method from section 5.3, but made it easier to measure in certain parts of the domain. All methods gave the same qualitative trends. This indicates that a new method for measuring the propagation speed of the pressure wave should be developed. The values of u_p in table 6.2 are therefore to be utilized with care, as more simulations are required to determine the actual value of u_p in the different cases.

The densities measured, ρ_b and ρ_u, are useful for checking that the simulations were done in proper order. The density of the unburned domain can be checked towards the fuel equivalence ratio to see if the intial field is correct. The expected value of ρ_b can also be checked towards the measured value as combustion of a fuel at a given ϕ can easily be predicted (through for example Gaseq). Both of these tests have been done to ensure that the simulations have a correct intialization and a correct combustion chemistry. It is also noted that a good indication of the correlation between the density and the fuel equivalence ratio is that ρ_u and ρ_b is decreasing with increasing ϕ (natural due to the definition of ϕ and an easy first test).

Measured parameters and theory

From the tables it is quite clear that the parameters are all influenced by the fuel equivalence ratio, as the theory indicate. The following trends were observed (in the given range of fuel equivalence ratios):

- Increasing fuel equivalence ratio, ϕ:
  - δ_f, ρ_b and ρ_u decreases.
  - u_b, S_L, u_p, ΔP, $\Delta P_{\min}$ and T_b increases.

The theory in section 2.2 suggest that the laminar flame speed will be influenced by the fuel equivalence ratio, namely by increasing with increasing temperature for the given fuel equivalence ratios, see fig. 2.3 (by the theory a

higher fuel equivalence ratio will lead to a higher flame temperature, until a certain ϕ). This first statement fits well with the results, as the laminar flame speed actually is increasing with increasing fuel equivalence ratio at $P = 1\,\text{atm}$. The theory also notes that with increasing pressure, the laminar flame speed will decrease. This second statement is not possible to check due to the fact that the simulations here is only for one pressure level, by given reasons in section 5.3.1.

The theory also relates the flame thickness with temperature (and pressure). With increasing temperature (increasing ϕ) (or pressure), the flame thickness is supposed to decrease. The results from the two dimensional simulations is in agreement with the theory.

The reference speed of sound in table 6.2 is given to compare the actual speed of sound at the given simulation conditions with the propagation speed of the pressure wave occuring after τ_i. It must be noted that there does not seem to be a relation between the propagation speed of the pressure wave and the speed of sound in the two dimensional simulations. The propagation speed of the pressure wave is much smaller than the speed of sound. The discussion in the previous paragraph indicate that the measurements should be done again using another method.

As expected from the theory T_b increases with increasing ϕ (see fig. 2.3 for the relevant ϕ's). As the temperature in the unburned domain is the same for all the cases ($T_u = 750\,\text{K}$) and the flame thickness decreases with increasing ϕ, the temperature gradient in the high ϕ domain is larger than in the low ϕ domain. The steeper temperature gradient induces a higher u_b.

6.1.2 Comparison of Analytical and Numerical Results

Here some simple comparisons of the analytical and numerical results will be presented. The relations found in section 4 will be repeated for overviews sake, and the actual comparative information will then be presented in tabular form. It is noted that there is only four sets of results to establish trends from, so the results should be regarded as uncertain and only as a preliminary study until more cases can be studied. A statistical analysis based on so few observations would be of little value.

It is important to understand that the comparison done in this chapter is based on an analytical approach in one dimension, as the analytical result of Talei et al. [37] of the axisymmetric case (see eq. (4.15)) was too complex to be of practical use. The comparison is done to investigate if the simple relations uncovered in section 4 can be used to estimate the parameters in a two dimensional simulation.

In section 4 three formulas were developed. Before τ_i the fluid expansion velocity, u_b, and the pressure difference between the unburned and burned domain, ΔP, was modeled by the following fairly simple relations:

$$u_b = S_L \left(\frac{\rho_u}{\rho_b} - 1 \right),$$

$$\Delta P = \rho S_L u_b.$$

After τ_i the pressure difference between the initial pressure and the minimum pressure, $\Delta P_{\min}$, was modeled in the following way:

$$\Delta P_{\min} = \rho u_p u_b.$$

If one assumes that $u_b = S_L \left(\frac{\rho_u}{\rho_b} - 1 \right)$ is valid after τ_i, and that $\rho \sim \rho_b$, this can be rewritten as:

$$\Delta P_{\min} = \rho_u u_p \left(1 - \frac{\rho_b}{\rho_u} \right) S_L.$$

In addition an analytical expression by Talei et al. [37] for the pressure difference between the initial pressure and the minimum pressure was presented in the following form:

$$P'(x,t) = -\rho_u c_b \left(1 - \frac{T_u}{T_b} \right) S_L.$$

These relations will now be investigated and discussed. The expressions for u_b, ΔP and $\Delta P_{\min}$ will be compared with the measured parameters, and a comparison of the ratios $\frac{\rho_b}{\rho_u}$ and $\frac{T_u}{T_b}$ will be performed. In tables 6.3 to 6.6 the relations are investigated by simple measures.

In table 6.3 a comparison between the pressure difference in the unburned and burned domain before τ_i from the numerical results and the analytical approach is presented. As mentioned in section 4.1 the linearization of ρ is expected to be by ρ_u before τ_i. In the project work of 2012 it was found that linearization with ρ_u gave the best result before τ_i. In table 6.3 ΔP is therefore calculated using only ρ_u. However, the results are far from the actual measurements. Another remark from the project work was that at low ϕ and high pressures the deviations were significantly higher than for the rest of the cases. Here a trend of increasing deviation with increasing ϕ can be seen. By the percentage deviations it is however clear that for the two dimensional simulations the analytical approximation of the pressure difference before τ_i is less reliable.

Table 6.3: Comparison of measured ΔP and calculated ΔP.

ϕ	$\Delta P_{\text{m.}}$	$\Delta P_{\text{c.}}$ [a]	ΔP [b]	% [c]
0.3	2.03	2.16	−0.13	−6.30
0.5	13.19	14.47	−1.28	−9.73
0.8	30.43	34.26	−3.83	−12.59
1.5	45.95	55.33	−9.38	−20.42

[*] Pressure differences is given in pascal, Pa.
[a] Calculated as $\Delta P = \rho_u S_L u_b$.
[b] Calculated as $\Delta P_{\text{m.}} - \Delta P_{\text{c.}}$.
[c] Calculated as $\frac{\Delta P}{\Delta P_{\text{m.}}} \times 100$.

Table 6.4: Comparison of measured u_b and calculated u_b.

ϕ	$u_{\text{b,m.}}$	$u_{\text{b,c.}}$ [a]	Δu_b [b]	% [c]
0.3	1.63	3.20	−1.57	−95.98
0.5	5.78	9.24	−3.46	−59.80
0.8	10.00	17.36	−7.35	−73.51
1.5	14.24	24.36	−10.12	−71.04

[a] Calculated as $u_b = S_L(\rho_u/\rho_b - 1)$.
[b] Calculated as $u_{\text{b,m.}} - u_{\text{b,c.}}$
[c] Calculated as $\frac{\Delta u_b}{u_{\text{b,m.}}} \times 100$.

Table 6.5: Comparison of measured ΔP_{min} and calculated ΔP_{min}.

ϕ	$\Delta P_{\text{min,m.}}$	$\Delta P_{\text{min,c.}}$ [a]	ΔP_{min} [b]	% [c]
0.3	-	-	-	-
0.5	28.8	32.7	−3.9	−13.5
0.8	145.3	49.7	95.6	65.8
1.5	297.9	256.5	41.4	13.9

[*] All values in pascal, Pa.
[a] Calculated as $\Delta P_{\text{min}} = \rho_b u_p u_b$.
[b] Calculated as $\Delta P_{\text{min,m.}} - \Delta P_{\text{min,c.}}$.
[c] Calculated as $\frac{\Delta P_{\text{min}}}{\Delta P_{\text{min,m.}}} \times 100$.

In table 6.4 the relation regarding the fluid expansion velocity before τ_i is compared with the numerical value. From the table it is quite clear that the deviations are rather large. The accuracy does not seem to follow a definite trend, and further investigations are needed to understand why this is. An indication is given in section 6.1.1, where the value of u_b is discussed. The values of u_b may be influenced by the relatively small domains, and simulations with larger domains (at adequat resolution) may give values of u_b which correspond better with the calculated values (as the calculated values are dependent on parameters which are less influenced by the domain).

In table 6.5 the pressure difference between the initial pressure and the minimum pressure *after* τ_i is investigated. A linearization of ρ has been done by ρ_b, as in the one dimensional simulations it was shown that $\rho \sim \rho_b$ was a somewhat more accurate and consistent linearization. Interestingly the formula for $\Delta P_{\min}$ only consists of three parameters, namely ρ_b, u_p and u_b. ρ_b was shown in section 6.1.1 to have the same values as expected from the theory (the same as in one dimension). As the expected values of $\Delta P_{\min}$ in the two dimensional cases are lower than the corresponding one dimensional simulations, the only way for eq. (4.9) to account for this is through u_b and/or u_p. Both of these values are also expected to have the same value as in the one dimensional simulations, which can be taken as an indication that the formula is to simple to be of practical use (no two dimensional effects are taken into account). The accuracy is decent for $\phi = 1.5$ and $\phi = 0.5$, but is poor for $\phi = 0.8$. The low accuracy for $\phi = 0.8$ seems to stem mainly from u_p which is low compared both to C_s and the other fuel equivalence ratios.

To summarize it is quite clear that the analytical expressions does not give a good impression of the pressure difference and fluid expansion velocity before τ_i or the pressure drop after τ_i. This is not unexpected and an obvious reason is that the one dimensional expressions does not implement the interactions between the flame that is observed in two dimensions (mainly the decreasing radius as the flame burns inwards). Simulations also indicate that u_b may be lower than expected due to boundary influence. The theory in section 4.2 remarks that classical acoustics dictates scaling in axisymmetric cases, and thereby it seems reasonable that some parameters are affected.

Also mentioned in section 4.2, is that Talei et al. [37] did develop a formula for the pressure fall after τ_i (eq. (4.15)). This formula is expected to have given a better approximation as it contains the effects the two dimensional simulations introduce. This formula is not used here due to its complexity.

In table 6.6 a comparison of the ratio between ρ_b and ρ_u, and T_u and T_b is performed. This is done in order to verify the equivalence between eqs. (4.9)

Table 6.6: Comparison of ρ_b/ρ_u and T_u/T_b.

ϕ	ρ_b/ρ_u	T_u/T_b	%[a]
0.3	0.495	0.469	5.19
0.5	0.407	0.376	7.69
0.8	0.354	0.317	10.49
1.5	0.347	0.308	11.14

[a] Calculated as $\frac{\rho_b/\rho_u - T_u/T_b}{\rho_b/\rho_u} \times 100$.

and (4.14). The temperature in the unburned domain was set by the initial conditions as $T_u = 750\,\mathrm{K}$. The general trend is an increasing deviation with increasing ϕ, yet the equivalence is reasonable. This indicates that there is not a huge difference between the two formulas, and it is interesting to see that such a simple approach as in section 4 may give approximetaly the same result as the more complicated approach in Talei et al. [37].

6.1.3 Comparison of Measured Parameters from One and Two Dimensional Simulations

Here the measured parameteres from one and two dimensional simulations will be compared. This is done to check the validity of the two dimensional simulations (through trends closely linked to the fuel equivalence ratio) and to quantify the similarites and dissimilarites and comment these.

The following general trends were observed in the one dimensional simulations (appendix B):

- Increasing fuel equivalence ratio, ϕ:
  - δ_f, ρ_b and ρ_u decreases.
  - u_b, S_L, u_p, ΔP and $\Delta P_{\min}$ increases.

In the two dimensional simulations the following trends were found (see section 6.1.1):

- Increasing fuel equivalence ratio, ϕ:
  - δ_f, ρ_b and ρ_u decreases.
  - u_b, S_L, u_p, ΔP and $\Delta P_{\min}$ increases.

The trends are the same for all the parameters. This is as expected, as the physical (qualitative) trends should not be affected by dimensional issues. This increases the validity of the two dimensional simulations by showing that the qualitative trends are maintained.

When it comes to the quantitative trends the expected result depends on the parameter. The densities (ρ_u and ρ_b) and the burned temperature (T_b) are expected to be the same for both one and two dimensional simulations due to their close link with the fuel equivalence ratio and the weak connection with other factors. u_b, S_L and u_p were expected to be approximetaly the same in both one and two dimension. By reasons given earlier (see sections 6.1.1 and 6.1.2), u_b and u_p are now expected to deviate significantly from the one dimensional results.

In table 6.7 a simple comparison of the one dimensional and two dimensional simulations is presented. The table is based on the tables in appendix C where a comparison has been done for each parameter. In the table only the percentage deviation is shown, so the reader is refered to appendix C if additional information is required. The subscripts m and c refer to if the parameters are measured or calculated, respectively.

Table 6.7: Comparison of one and two dimensional simulations in %.

ϕ	0.3	0.5	0.8	1.5
$u_{b,m}$	47.42	36.69	42.40	40.94
$u_{b,c}$	−5.26	−1.20	0.69	−0.33
δ_f	47.57	70.29	63.42	62.76
ρ_u	2.60	1.36	−0.30	−1.25
ρ_b	−0.10	0.08	0.00	0.14
S_L	0.16	1.03	0.23	−2.46
u_p	-	95.85	96.01	84.19
ΔP_m	49.88	41.89	48.23	49.61
ΔP_c	47.19	37.41	42.52	39.58
$\Delta P_{\mathrm{min,m}}$	-	96.53	89.50	83.31
$\Delta P_{\mathrm{min,c}}$	-	96.31	95.80	81.91
T_b	−1.89	−1.04	1.25	2.09

A lot of information can be drawn from table 6.7 (and appendix C). In the next few paragraphs the results in these tables will be presented and discussed. The investigation will not look at the relation between the measured and calculated parameters isolated in one and two dimensions, as these were handled in section 6.1.2, but will focus on the comparison of one and two dimensional results.

The fluid expansion velocity is investigated both as a measured value, $u_{b,m}$ and a calculated value from eq. (4.8), $u_{b,c}$. In the case of the measured value the deviation is rather large for all values of ϕ, but the absolute deviation is fairly constant. Simulations indicate that u_b may be lower than expected due to boundary influence, such that the deviation between the one and two dimensional results will increase. (See section 6.1.1 for a discussion on u_b.) In the case of the calculated value the deviation is much smaller. This is contributed mainly to the factors in the formula (ρ_u, ρ_b and S_L), which were expected to have small deviations. It is noted that the percentage deviation is rather large for $\phi = 0.3$, but in table C.2 it can be seen that the deviation for all cases is of the same order (the smaller value of u_b makes the relative error larger). These results shows that a two dimensional simulation can give the expected fluid expansion velocity in a one dimensional simulation using eq. (4.8).

The flame width is generally thinner in two dimensions than one dimension. A theory is that the decreasing radius influences the flame width, but this claim is in need of thorough investigation to be confirmed. The deviation is rather large and there does not seem to be a clear trend to increasing/decreasing deviation with fuel equivalence ratio.

The densities, ρ_u and ρ_b, and burned temperature, T_b have, as expected, a very low deviation. This is contributed to the strong link between the fuel equivalence and the density and burned temperature (as discussed in section 6.1.1). That these values have a low deviation only serves to confirm that the simulations have been done under the correct conditions.

The propagation speed of the flame shows very good agreement between the one and two dimensional simulations. One has to be careful as this is a parameter which changes value in the two dimensional simulations due to the scaling effect. As the flame burns inwards S_L will increase. The value measured and presented here is measured as early after initialization as possible to ensure comparability with the one dimensional simulations.

The propagation speed of the pressure wave occuring at annihilation is showing a remarkable deviation. u_p is much lower in the two dimensional cases. The reasons for this probably lies in the uncertanties described in section 6.1.1. It is noted that $\phi = 0.3$ is not investigated as the value was not possible to measure

due to the resolution of the solution files (and tools used to measure the value).

The pressure difference before τ_i is investigated both as a measured and calculated value. The agreement is better for the calculated value, but is poor for both cases. This is related to the parameters used in the formulas. As discussed in section 6.1.1 some parameters have a better agreement. A formula where the parameteres in one dimension and two dimensions have a good agreement, will consequently give a good agreement. There is no trend to the deviations in either case.

The pressure drop at annihilation is also investigated both as a measured and calculated value. It is noted that $\phi = 0.3$ is not investigated for this parameter as the value could not be measured correctly. The deviations is in approximetaly the same range, and is very large for both. A trend of decreasing deviation with increasing fuel equivalence ratio can be seen. $\Delta P_{\min}$ was expected to be smaller in two dimensions (see section 4.3, Talei et al. [37]). It is clear from the results that this is the case. To determine the driving parameters for the pressure drop, and thereby be able to predict the pressure drop by dimensionality (one, two or three dimensions), requires more in depth analysis of the problem. Investigations regarding boundary influence, heat release related to the pressure drop, and so forth has to be performed.

6.2 Three Dimensional Simulations

In this section the results from the three dimensional simulations will be presented. In the introduction it was specified that this part of the thesis would only be devoted time if time allowed it. As the work on the thesis has progressed it has been clear that a thorough study in three dimensions was not possible due to time issues. There was not enough time to alter the source code to the desired effect (the boundary problems would need to be adressed for the final boundary), and the simulations would be unfeasible as the simulation time would be very large (minimum 20+ days on roughly 140 cores).

This part of the thesis was therefore restricted to the initialization of a spherical flame in a cubic domain. This set-up models the actual annihilation of a inwards burning gas bubble, and is consequently the most interesting case as it is closest to reality (in a gas turbine combustion chamber). In fig. 6.2 the temperature field of an inwards burning sphere (halved) at initialization is presented.

The work consisted mainly of changing the source files to incorporate the spherical flame. The alterations were mostly done in init_flame.f90, which can be found in appendices D and E.

As only the initialization of the flame is done, there are no actual results, but a good basis for further investigation is laid. As one can see in fig. 6.2 the initialization of the spherical flame is correct, such that the main thing left is to correct the boundary problems in update_L.f90. It is however recommended that the boundary conditions in update_L.f90 are made from scratch (and thereby customized to this problem) to ensure that the physicality of the problem is maintained.

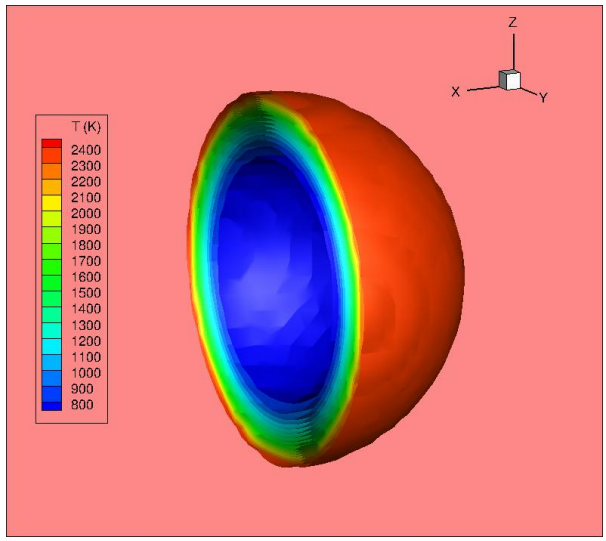

Figure 6.2: Temperature field of an inwards burning sphere (halved) at initialization of a three dimensional simulation.

7 Conclusions

Direct Numerical Simulations (DNS) of laminar compressible reactive flows have been investigated. Simulations of two dimensional laminar imploding circular flame fronts have been performed the main focus of thesis. Also one dimensional simulations of laminar opposing flame fronts have been performed to establish modeling conditions for the two dimensional simulations, evaluate the boundary influence on the simulations and provide comparable simulation results. In addition a pre-study for three dimensional simulation of an inwards burning sphere of fuel has been done.

The DNS code (S3D) for two dimensional imploding flame fronts was modified to work under given conditions. It was found that the axisymmetric flame showed a symmetric behaviour, although a thorough investigation regarding the boundary conditions is recommended to validate this fully.

Through one dimensional simulations modeling conditions for two dimensional simulations were found. This made it possible to run the simulations in a reasonable amount of time. It was, however, also discovered through one dimensional simulations that the influence of the boundary on the solution may be large. This implies further investigation through simulations both in one and two dimensions with special focus on boundary influence on the solution.

As expected a pressure wave propagates from the center of the domain after annihilation (after τ_i). Further investigation is nedeed to verify the claim that the annihilation event will instigate several pressure waves. Further investigation is also needed to to verify the claim that this/these pressure wave(s) will propagate at the speed of sound.

A method for measuring the propagation speed of the pressure wave after τ_i needs to be developed. The current method(s) showed that u_p was much smaller than C_s. The hypothesis that u_p equals C_s needs further work to be confirmed as the method(s) used seems insufficient.

It was indicated that the fluid expansion velocity, u_b, will be equal in one and two dimensions if the influence of the boundaries are at a minimum (that is, when the radius of the flame is large, and the distance from the boundary to the flame front is sufficient). It is suggested to investigate this by simulating on a larger domain.

The following trends were found for the two dimensional simulations:

- With increasing fuel equivalence ratio:
  - τ_f, ρ_b and ρ_u decreases.

– u_b, S_L, u_p, ΔP, $\Delta P_{\min}$ and T_b increases.

This coincides with the trends in the one dimensional simulations, and is consistent with the given theory.

Three simple relations were developed in section 4 (eqs. (4.6), (4.8) and (4.9)). These relations were then compared with the measured numerical results and gave the following:

- Equation (4.6) is less reliable in two dimensions than in one dimension.
- Equation (4.8) gave large deviations from the measured value. Here the measured value are under question due to boundary issues (small domain). A simulation on a larger domain indicates that the measured u_b may equal the calculated u_b if the domain length is increased, but further investigation is needed to conclude.
- Equation (4.9) gave a poor representation of the measured ΔP.

The relations in general does not give a good impression of the corresponding measured values in two dimensions. The simplifications in the analytical approach does not take account of the two dimensional effects (like interactions at the flame front and the decreasing circumference of the flame front).

The comparison between one and two dimensional results mainly show that there are many variables in interplay, and that based on the current data an in depth analysis of the physics of the interactions in the two dimensional simulations will be speculations. It is rather noted that to fully understand the annihilation process, and the consequent pressure drop, several simulations have to be run (same conditions, proper investigation of boundaries, etc.). Especially the parameters u_p, u_b and $\Delta P_{\min}$ are under scrutiny and should be investigated thorougly.

In the three dimensional simulations the only conclusion which can be drawn is that the boundary conditions in update_L.f90 have to be revised such that they are symmetric in all three dimensions.

8 Suggestions for further work

The following is suggested to continue the study of sound generation by flame annihilation in a gas turbine combustion chamber:

- Study the boundary influence on the annihilation event. This is motivated by a simulation which indicated that the pressure drop after τ_i may have been affected by the boundary conditions and a theory of Nils E. Haugen which states that the fluid expansion velocity should be equal in one and two dimensions if the radius of the flame is large enough. To map the situation a one dimensional pre-study should be done. Simulations with longer domains (for example 5 cm), compared with the results of now should give an indication of the boundary influence. The one dimensional pre-study was done as two dimensional simulations takes more time and are considerably more costly. Based on the results of the one dimensional pre-study, simulations on larger domains in two dimensions in all cases have to be considered. It is important to have an adequat inital distance from the boundary to the flame and an adequat radius of the flame. This is to minimize the boundary influence on the early simulation stages and to ensure that two dimensional interactions have as little influence as possible on the results. Based on these studies an evaluation of the results in this thesis should be performed.

- A new method for measuring the propagation speed of the pressure wave after τ_i needs to be developed. The current methods are boundary dependent and does not give consistent results.

- Extend the study of one dimensional combustion by introducing more pressure and fuel equivalence ratio levels. The motivation is to study the effect of the surrounding pressure and the fuel equivalence ratio. A study of simple chemistry representation compared to the detailed is also encouraged for these new levels.

- Extend the study of two dimensional combustion by introducing more pressure and fuel equivalence ratio levels. Here it is first and foremost thought of as a continuation of the work done in this thesis (do simulations for pressure levels 5 and 10 atm with the same fuel equivalence ratios), but also to extend it further, as in the one dimensional simulations of the project work of fall 2012, with both detailed and simple chemistry representation.

- Continue work on the three dimensional inwards burning sphere to model annihilation of the fuel droplet itself. The initialization of this droplet is completed, and the remaining work is to modify update_L.f90 such that it is symmetric in all three directions and then run simulations for given cases, and perform measurements as for the one and two dimensional simulations. These simulations will model the actual situation (in the gas turbine combustion chamber) in a much better way, and hopefully give a metter measure of the actual pressure wave amplitude and frequency caused by flame annihilaion in a gas turbine combustion chamber.

- Turbulence studies in two and three dimensions. These studies are to determine the influence of turbulence on the parameters, with special focus on the pressure drop after τ_i. The S3D code are capable of turbulence studies, but the simulation conditions (domain length, number of grid points, timestep, etc.) have to be modified to account for the increased complexity of the problem.

- The theory that several pressure waves are to be formed in two and three dimensions should be investigated. This implies running simulations longer than annihilation, and observe if these pressure waves occur. If they do not occur, the question "why do they not occur" should be asked. This question is then expected to be closely linked with the boundary influence, and larger domain studies seems (by todays knowledge) to be of the essence.

- Investigate the possibility of using eq. (4.15) from Talei et al. [37] in the analytical comparison with the measured parameters from the numerical simulations. The most efficient way would seem to implement eq. (4.15) into the S3D code.

- Investigate boundary influence as a consequence of the boundary shape. In Talei et al. [38] the boundary used in the axisymmetric case has a circular shape, while in this thesis the domain has the shape of a square.

References

[1] World Energy Outlook 2012. http://www.worldenergyoutlook.org/publications/weo-2012/. Accessed 10/06/2013.

[2] Tecplot 360. http://www.tecplot.com.

[3] J. T. Agnew and L. B. Graiff. The pressure dependence of laminar burning velocity by the spherical bomb method. *Combustion and Flame*, 5(0):209 – 219, 1961. ISSN 0010-2180. doi: 10.1016/0010-2180(61)90099-2. URL http://www.sciencedirect.com/science/article/pii/0010218061900992.

[4] G. K. Batchelor. *An Introduction to Fluid Dynamics*. Cambridge University Press, Cambridge, third edition, 2000.

[5] Michael J. Brear, Frank Nicoud, Mohsen Talei, Alexis Giauque, and Evatt R. Hawkes. Disturbance energy transport and sound production in gaseous combustion. *Journal of Fluid Mechanics*, 707:53–73, 2012. doi: 10.1017/jfm.2012.264. URL http://dx.doi.org/10.1017/S0022112012002649.

[6] J. H. Chen, A. Choudhary, B. de Supinski, M. DeVries, E. R. Hawkes, S. Klasky, W. K. Liao, K. L. Ma, J. Mellor-Crummey, N. Podhorszki, R. Sankaran, S. Shende, and C. S. Yoo. Terascale direct numerical simulations of turbulent combustion using s3d. *Computational Science & Discovery*, 2(1):015001, 2009. URL http://stacks.iop.org/1749-4699/2/i=1/a=015001.

[7] Paul Clavin and Eric D. Siggia. Turbulent premixed flames and sound generation. *Combustion Science and Technology*, 78(1-3):147–155, 1991. doi: 10.1080/00102209108951745. URL http://www.tandfonline.com/doi/abs/10.1080/00102209108951745.

[8] A. E. Dahoe. Laminar burning velocities of hydrogen-air mixtures from closed vessel gas explosions. *Journal of Loss Prevention in the Process Industries*, 18(3):152 – 166, 2005. ISSN 0950-4230. doi: 10.1016/j.jlp.2005.03.007. URL http://www.sciencedirect.com/science/article/pii/S0950423005000392.

[9] A. P. Dowling. *Modern Methods in Analytical Acoustics*, chapter Thermoacoustic Sources and Instabilities.

[10] A. P. Dowling. The calculation of thermoacoustic oscillations. *Journal of Sound and Vibration*, 180(4):557 – 581, 1995. ISSN 0022-460X. doi: 10.1006/jsvi.1995.0100. URL http://www.sciencedirect.com/science/article/pii/S0022460X85701009.

[11] A. P. Dowling and S. Hubbard. Instability in lean premixed combustors. *Proceedings of the Institution of Mechanical Engineers, Part A: Journal of Power and Energy*, 214:317–332, 2000. doi: 10.1243/0957650001537903. URL http://pia.sagepub.com/content/214/4/317.

[12] Isadore L. Drell and Frank E. Belles. Survey of hydrogen combustion properties. 1958. URL http://naca.larc.nasa.gov/reports/1958/naca-report-1383.

[13] A. Gruber, R. Sankaran, E. R. Hawkes, and J. H. Chen. Turbulent flame wall interaction: a direct numerical simulation study. *Journal of Fluid Mechanics*, 658:5–32, 2010. doi: 10.1017/S0022112010001278. URL http://dx.doi.org/10.1017/S0022112010001278.

[14] Andrea Gruber. *Direct Numerical Simulation Of Turbulent Combustion Near Solid Surfaces*. PhD thesis, Norwegian University of Science and Technology, Department of Energy and Process Engineering, 2006.

[15] L. Guichard, Julien Reveillon, and R. Hauguel. Direct numerical simulation of statistically stationary one- and two-phase turbulent combustion: A turbulent injection procedure. *Flow, Turbulence and Combustion*, 73:133–167, 2004. ISSN 1386-6184. URL http://dx.doi.org/10.1023/B:APPL.0000049273.27776.f5. 10.1023/B:APPL.0000049273.27776.f5.

[16] A. K. Gupta. Gas turbine combustion: Prospects and challenges. *Energy Conversion and Management*, 38(10-13):1311–1318, 1997. ISSN 0196-8904. doi: 10.1016/S0196-8904(96)00160-4. URL http://www.sciencedirect.com/science/article/pii/S0196890496001604. International Symposium on Advance Energy Conversion Systems and Related Technologies.

[17] Evatt R. Hawkes and Jacqueline H. Chen. Comparison of direct numerical simulation of lean premixed methane air flames with strained laminar flame calculations. *Combustion and Flame*, 144(1-2):112 – 125, 2006. ISSN 0010-2180. doi: 10.1016/j.combustflame.2005.07.002. URL http://www.sciencedirect.com/science/article/pii/S0010218005001793.

[18] Evatt R. Hawkes, Ramanan Sankaran, James C. Sutherland, and Jacqueline H. Chen. Direct numerical simulation of turbulent combustion: fundamental insights towards predictive models. *Journal of Physics: Conference Series*, 16(1):65, 2005. URL http://stacks.iop.org/1742-6596/16/i=1/a=009.

[19] H. M. Heravi, A. Azarinfar, S. I. Kwon, P. J. Bowen, and N. Syred. Determination of laminar flame thickness and burning velocity of methane-air mixture. Third European Combustion Meeting ECM, 2007.

[20] R. Hilbert, F. Tap, H. El-Rabii, and D. Thévenin. Impact of detailed chemistry and transport models on turbulent combustion simulations. *Progress in Energy and Combustion Science*, 30(1):61 – 117, 2004. ISSN 0360-1285. doi: 10.1016/j.pecs.2003.10.001. URL http://www.sciencedirect.com/science/article/pii/S036012850300073X.

[21] S. Kato, T. Fujimori, A. P. Dowling, and H. Kobayashi. Effect of heat release distribution on combustion oscillation. *Proceedings of the Combustion Institute*, 30(2):1799 – 1806, 2005. ISSN 1540-7489. doi: 10.1016/j.proci.2004.08.154. URL http://www.sciencedirect.com/science/article/pii/S0082078404002061.

[22] Jacob J. Keller and George F. McLaughlin. Thermoacoustic oscillations in combustion chambers of gas turbines. *AIAA Journal*, 33(12):2280–2287, 1995. doi: 10.2514/3.12980. URL http://arc.aiaa.org/doi/abs/10.2514/3.12980.

[23] Jakob J. Keller. Nonlinear self-excited acoustic oscillations within fixed boundaries. *Journal of Fluid Mechanics*, 123:267–281, 1982. doi: 10.1017/S002211208200305X. URL http://dx.doi.org/10.1017/S002211208200305X.

[24] Juan Li, Zhenwei Zhao, Andrei Kazakov, and Frederick L. Dryer. An updated comprehensive kinetic model of hydrogen combustion. *International Journal of Chemical Kinetics*, 36(10):566–575, 2004. ISSN 1097-4601. doi: 10.1002/kin.20026. URL http://dx.doi.org/10.1002/kin.20026.

[25] M. J. Lighthill. On sound generated aerodynamically. i. general theory. *Proceedings of the Royal Society of London. Series A. Mathematical and Physical Sciences*, 211(1107):564–587, 1952. doi: 10.1098/rspa.1952.0060. URL http://rspa.royalsocietypublishing.org/content/211/1107/564.abstract.

[26] A. N. Lipatnikov and J. Chomiak. Turbulent flame speed and thickness: phenomenology, evaluation, and application in multi-dimensional simulations. *Progress in Energy and Combustion Science*, 28(1):1 – 74, 2002. ISSN 0360-1285. doi: 10.1016/S0360-1285(01)00007-7. URL http://www.sciencedirect.com/science/article/pii/S0360128501000077.

[27] Parviz Moin and Krishnan Mahesh. Direct numerical simulation: A tool in turbulence research. *Annual Review of Fluid Mechanics*, 30(1):539–578, 1998. doi: 10.1146/annurev.fluid.30.1.539. URL http://www.annualreviews.org/doi/abs/10.1146/annurev.fluid.30.1.539.

[28] Chris Morley. Gaseq. http://www.gaseq.co.uk/.

[29] M. K. Myers. Transport of energy by disturbances in arbitrary steady flows. *Journal of Fluid Mechanics*, 226:383–400, 1991. doi: 10.1017/S0022112091002434. URL http://dx.doi.org/10.1017/S0022112091002434.

[30] N. Peters. Fifteen lectures on laminar and turbulent combustion. Ercoftac Summer School, September 14-28, 1992, Aachen, Germany, RTWH Aachen.

[31] Thierry Poinsot and Denis Veynante. *Theoretical and Numerical Combustion*. R. T. Edwards, Philadelphia, second edition, 2005.

[32] Xiao Qin, Hideaki Kobayashi, and Takashi Niioka. Laminar burning velocity of hydrogen air premixed flames at elevated pressure. *Experimental Thermal and Fluid Science*, 21(1-3):58 – 63, 2000. ISSN 0894-1777. doi: 10.1016/S0894-1777(99)00054-0. URL http://www.sciencedirect.com/science/article/pii/S0894177799000540.

[33] C. D. Rakopoulos, G. M. Kosmadakis, and E. G. Pariotis. Evaluation of a combustion model for the simulation of hydrogen spark-ignition engines using a CFD code. *International Journal of Hydrogen Energy*, 35 (22):12545 – 12560, 2010. ISSN 0360-3199. doi: 10.1016/j.ijhydene.2010.09.002. URL http://www.sciencedirect.com/science/article/pii/S0360319910017891. <ce:title>Bio-Ethanol and Other Renewable Sources and Reforming Process for Sustainable Hydrogen Production</ce:title>.

[34] H. I. H. Saravanamuttoo, G. F. C. Rogers, H. Cohen, and P. V. Straznicky. *Gas Turbine Theory*. Pearson Education Limited, Essex, England, sixth edition, 2009.

[35] W. C. Strahle. Combustion noise. *Progress in Energy and Combustion Science*, 4:157–176, 1978.

[36] Jochen Ströhle and Tore Myhrvold. An evaluation of detailed reaction mechanisms for hydrogen combustion under gas turbine conditions. *International Journal of Hydrogen Energy*, 32(1):125 – 135, 2007. ISSN 0360-3199. doi: 10.1016/j.ijhydene.2006.04.005. URL http://www.sciencedirect.com/science/article/pii/S0360319906001716.

[37] Mohsen Talei, Michael J. Brear, and Evatt R. Hawkes. Sound generation by laminar premixed flame annihilation. *Journal of Fluid Mechanics*, 679: 194–218, 2011. doi: 10.1017/jfm.2011.131. URL http://dx.doi.org/10.1017/S0022112011001315.

[38] Mohsen Talei, Michael John Brear, and Evatt Robert Hawkes. A parametric study of sound generation by premixed laminar flame annihilation. *Combustion and Flame*, 159(2):757 – 769, 2012. ISSN 0010-2180. doi: 10.1016/j.combustflame.2011.08.025. URL http://www.sciencedirect.com/science/article/pii/S0010218011002744.

[39] Mohsen Talei, Ewatt R. Hawkes, and Michael J. Brear. A direct numerical simulation study of frequency and lewis number effects on sound generation by two-dimensional forced laminar premixed flames. *Preprint submitted to 33rd combustion symposium*, July 16, 2012.

[40] H. Tennekes and J. L. Lumley. *A First Course in Turbulence*. The MIT Press, Cambridge, first edition, 1972.

[41] Stephen R. Turns. *An Introduction to Combustion: Concepts and Applications*. McGraw-Hill Higher Education, Singapore, second edition, 2006.

[42] Sebastian Verhelst and Thomas Wallner. Hydrogen-fueled internal combustion engines. *Progress in Energy and Combustion Science*, 35(6):490 – 527, 2009. ISSN 0360-1285. doi: 10.1016/j.pecs.2009.08.001. URL http://www.sciencedirect.com/science/article/pii/S0360128509000422.

[43] J. Warnatz, U. Maas, and R. W. Dibble. *Combustion, Physical and Chemical Fundamentals, Modeling and Simulation, Experiments, Pollutant Formation*.

[44] C. M. White, R. R. Steeper, and A. E. Lutz. The hydrogen-fueled internal combustion engine: a technical review. *International Journal of Hydrogen Energy*, 31(10):1292 – 1305, 2006. ISSN 0360-3199. doi: 10.1016/j.ijhydene.

2005.12.001. URL http://www.sciencedirect.com/science/article/pii/S0360319905003721.

[45] F. M. White. *Fluid Mechanics*. McGraw-Hill Book Company, New York, sixth edition, 2008.

A Analytical Approach

Here the full derivations of the simple relations in section 4 are given. First the two relations for the time before τ_i, then the pressure relation for the time after τ_i are presented.

Pressure before τ_i
In a coordinate system following one of the flame fronts, eq. (4.5) can be written as:

$$\frac{Du}{Dt} = -\frac{1}{\rho}\frac{\partial P}{\partial x}. \tag{A.1}$$

As the area of interest is over the flame front, the following approximations are done:

$$\frac{Du}{Dt} \sim -\frac{u_b}{\tau_f}, \tag{A.2a}$$

$$-\frac{1}{\rho}\frac{\partial P}{\partial x} \sim -\frac{1}{\rho}\frac{\Delta P}{\delta_f}, \tag{A.2b}$$

where u_b is the fluid expansion velocity, $\tau_f = \frac{\delta_f}{S_L}$ is the time scale for the propagation of the flame front, δ_f is the width of the flame, and S_L is the flame propagation velocity. The density, ρ, is expected to be linearized by the density of the unburned region, ρ_u. An approximation of eq. (A.1) then reads:

$$\frac{u_b}{\tau_f} = \frac{1}{\rho}\frac{\Delta P}{\delta_f}, \tag{A.3}$$

which with some algebra and the definition of the time scale, $\tau_f = \frac{\delta_f}{S_L}$, give the relation:

$$\Delta P = \rho \delta_f \frac{u_b}{\tau_f} = \rho S_L u_b. \tag{A.4}$$

Fluid expansion velocity before τ_i
To develop an explicit expression for u_b, eq. (4.4) is manipulated in the same way as eq. (4.5). The area of interest is still over the flame front, and the following approximations are done:

$$\frac{\partial \rho}{\partial t} \sim \frac{\Delta \rho}{\tau_f}, \tag{A.5a}$$

$$u\frac{\partial \rho}{\partial x} \sim u_b \frac{\Delta \rho}{\delta_f}, \tag{A.5b}$$

$$\rho \frac{\partial u}{\partial x} \sim -\rho \frac{u_b}{\delta_f}, \tag{A.5c}$$

where $\Delta\rho = \rho_u - \rho_b$ and u is linearized as u_b as there is no expansion velocity in the unburned region, i.e. $u_u = 0$. It is expected that ρ will be linearized as ρ_u. The approximation of eq. (4.4) then reads:

$$\frac{\Delta\rho}{\tau_f} + u_b \frac{\Delta\rho}{\delta_f} - \rho \frac{u_b}{\delta_f} = 0. \tag{A.6}$$

Some rearrangements and the definition $\tau_f = \frac{\delta_f}{S_L}$ gives:

$$u_b \left(\rho - \Delta\rho\right) = S_L \Delta\rho. \tag{A.7}$$

If it is assumed that $\rho \sim \rho_u$, the following relation is acquired:

$$u_b = S_L \left(\frac{\rho_u}{\rho_b} - 1\right). \tag{A.8}$$

Pressure after τ_i
After τ_i the terms in eq. (4.5) are approximated by:

$$\frac{\partial u}{\partial t} \sim -\frac{u_b}{\tau_a}, \tag{A.9a}$$

$$u \frac{\partial u}{\partial x} \sim -u_b \frac{u_b}{\delta_a}, \tag{A.9b}$$

$$-\frac{1}{\rho}\frac{\partial P}{\partial x} \sim -\frac{1}{\rho}\frac{\Delta P}{\delta_a}, \tag{A.9c}$$

where τ_a and δ_a are the time scale and length scale based on the propagation of the pressure wave, respectively. An approximation of eq. (4.5) then reads:

$$\frac{u_b}{\tau_a} + u_b \frac{u_b}{\delta_a} = \frac{1}{\rho}\frac{\Delta P}{\delta_a}. \tag{A.10}$$

Some algebra and the definition $\tau_a = \frac{\delta_a}{u_p}$ then reveals:

$$u_b + u_b \frac{u_b}{u_p} = \frac{1}{\rho}\frac{\Delta P}{u_p}. \tag{A.11}$$

As $u_b \frac{u_b}{u_p} \ll u_b$, eq. (A.11) then becomes:

$$u_b = \frac{1}{\rho} \frac{\Delta P}{u_p}. \tag{A.12}$$

Some rearrangments gives the relation between the pressure change and density, speed of sound and fluid expansion velocity:

$$\Delta P = \rho u_p u_b. \tag{A.13}$$

B Measured Parameters from One Dimensional Simulations

Here the measured parameters from the one dimensional simulations performed in the candidate's project work of fall 2012 are presented. These are used for comparison with the two dimensional simulations in this thesis. The measurements are done in approximetaly the same way as the two dimensional simulations (as far as possible) to ensure comparability.

Table B.1: Measured parameters.

ϕ	u_b (m/s)	δ_f (10^{-4} m)	ρ_b (kg/m^3)	ρ_u (kg/m^3)	S_L (m/s)
0.3	3.10	8.117	0.213 90	0.420 68	3.141
0.5	9.13	8.659	0.162 83	0.394 63	6.415
0.8	17.36	6.402	0.127 14	0.360 32	9.528
1.5	24.11	5.263	0.102 97	0.301 31	12.604

Table B.2: Measured parameters 2.

ϕ	C_s (m/s)[a]	u_p (m/s)	ΔP (Pa)	$\Delta P_{\min}$ (Pa)	T_b (K)
0.3	788.6	604.5	4.05	268.3	1569.15
0.5	897.0	848.2	22.70	829.2	1974.06
0.8	1010.8	976.6	58.78	1383.9	2397.63
1.5	1120.5	1092.5	91.19	1784.9	2487.76

[a] The products speed of sound found from Gaseq with adiabatic temperature and composition at constant $P = 1\,\text{atm}$ and initial temperature $T = 750\,\text{K}$.

C Comparison of Measured Parameters from One and Two Dimensional Simulations

Here the full tables of comparison between the one and two dimensional simulations are presented. These serve as background information for the extract table in section 6.1.3 (table 6.7).

The tables cover each parameter presented in section 5.3. In the cases where the parameter is calculated this is also covered.

The tables are calculated as following. Column two is the one dimensional value of the specific parameter, and column three is the two dimensional value. In column four column 3 is subtracted from column 2 to get the absolute difference betweeen the two. In column 5 the absolute difference is divided with column 2 (and then multiplied with 100) to get the percentage deviation relative to the one dimensional simulation.

Table C.1: Comparison of measured u_b.

ϕ	$u_{b,1D}$	$u_{b,2D}$	Δu_b	%
0.3	3.10	1.63	1.47	47.42
0.5	9.13	5.78	3.35	36.69
0.8	17.36	10.00	7.36	42.40
1.5	24.11	14.24	9.87	40.94

Table C.2: Comparison of calculated u_b.

ϕ	$u_{b,1D}$	$u_{b,2D}$	Δu_b	%
0.3	3.04	3.20	−0.16	−5.26
0.5	9.13	9.24	−0.11	−1.20
0.8	17.48	17.36	0.12	0.69
1.5	24.28	24.28	−0.08	−0.33

Table C.3: Comparison of δ_f.

ϕ	$\delta_{f,1\mathrm{D}}$	$\delta_{f,2\mathrm{D}}$	$\Delta\delta_f$	%
0.3	8.117	4.256	3.861	47.57
0.5	8.659	2.573	6.086	70.29
0.8	6.402	2.342	4.060	63.42
1.5	5.263	1.960	3.303	62.76

Table C.4: Comparison of ρ_u.

ϕ	$\rho_{u,1\mathrm{D}}$	$\rho_{u,2\mathrm{D}}$	$\Delta\rho_u$	%
0.3	0.213 90	0.208 34	0.0056	2.60
0.5	0.162 83	0.160 61	0.0022	1.36
0.8	0.127 14	0.127 52	−0.0004	−0.30
1.5	0.102 97	0.104 26	−0.0013	−1.25

Table C.5: Comparison of ρ_b.

ϕ	$\rho_{b,1\mathrm{D}}$	$\rho_{b,2\mathrm{D}}$	$\Delta\rho_b$	%
0.3	0.420 68	0.421 09	−0.0004	−0.10
0.5	0.394 63	0.394 30	0.0003	0.08
0.8	0.360 32	0.360 32	0	0.00
1.5	0.301 31	0.300 90	0.0004	0.14

Table C.6: Comparison of S_L.

ϕ	$S_{L,1\mathrm{D}}$	$S_{L,2\mathrm{D}}$	ΔS_L	%
0.3	3.141	3.136	0.005	0.16
0.5	6.415	6.349	0.066	1.03
0.8	9.528	9.506	0.022	0.23
1.5	12.604	12.914	−0.31	−2.46

Table C.7: Comparison of u_p.

ϕ	$u_{p,1D}$	$u_{p,2D}$	Δu_p	%
0.3	604.5	-	-	-
0.5	848.2	35.2	813.0	95.85
0.8	976.6	39.0	937.6	96.01
1.5	1092.5	172.7	919.8	84.19

Table C.8: Comparison of measured ΔP.

ϕ	ΔP_{1D}	ΔP_{2D}	ΔP	%
0.3	4.05	2.03	2.02	49.88
0.5	22.70	13.19	9.51	41.89
0.8	58.78	30.43	28.35	48.23
1.5	91.19	45.95	45.24	49.61

Table C.9: Comparison of calculated ΔP.

ϕ	ΔP_{1D}	ΔP_{2D}	ΔP	%
0.3	4.09	2.16	1.93	47.19
0.5	23.12	14.47	8.65	37.41
0.8	59.60	34.26	25.34	42.52
1.5	91.57	55.33	36.24	39.58

Table C.10: Comparison of measured $\Delta P_{\min}$.

ϕ	$\Delta P_{\min,1D}$	$\Delta P_{\min,2D}$	$\Delta P_{\min}$	%
0.3	268.3	-	-	-
0.5	829.2	28.8	800.4	96.53
0.8	1383.9	145.3	1238.6	89.50
1.5	1784.9	297.9	−1487.0	83.31

Table C.11: Comparison of calculated $\Delta P_{\min}$.

ϕ	$\Delta P_{\min,1D}$	$\Delta P_{\min,2D}$	$\Delta P_{\min}$	%
0.3	406.1	-	-	-
0.5	885.9	32.7	853.2	96.31
0.8	1183.1	49.7	1133.4	95.80
1.5	1417.9	256.5	1161.4	81.91

Table C.12: Comparison of T_b.

ϕ	$T_{b,1D}$	$T_{b,2D}$	ΔT_b	%
0.3	1569.15	1598.80	-29.65	-1.89
0.5	1974.06	1994.59	-20.53	-1.04
0.8	2397.63	2367.59	30.04	1.25
1.5	2487.76	2435.71	52.05	2.09

D Fortran Source Code - Set C-profile

Attached is some of the source code in init_flame.90 which initializes many of the characteristics of the flame. To not include to much code in this thesis, the code given is a bare minimum of the actual code.

Here the code for initializing the flame itself in one, two and three dimensions is included (meeting flame fronts, circular planar flame and spherical flame under executable statements in subroutine set_c_prof).

```
!=======================================================================
   subroutine set_c_prof(c,tan_alpha,trans_width,x_centre,
                         y_centre,z_centre,rod_width,i_fgeo)
!=======================================================================
 ! prescribes spatial c-variation
 ! Evatt Hawkes July 2003, modified by Andrea Gruber 2005/03/01
!-----------------------------------------------------------------------
   use topology_m
   use param_m, only : nx,ny,nz,nx_g,ny_g,nz_g,periodic_x,
                       periodic_y,periodic_z,vary_in_x,
                       vary_in_y,vary_in_z
   use grid_m, only : xmax,xmin,delx,ymax,ymin,dely,
                      zmax,zmin,delz,x,y,z
   use bc_m
   use reference_m, only : l_ref

   implicit none
!-----------------------------------------------------------------------
 ! declarations passed
   integer, intent(in)  :: i_fgeo      !flame geometry flag
   real,    intent(in)  :: tan_alpha   !tan of v-flame half angle
   real,    intent(in)  :: trans_width !thickness of c profile
   real,    intent(in)  :: x_centre    !centre in x-direction
   real,    intent(in)  :: y_centre    !centre in y-direction
   real,    intent(in)  :: z_centre    !centre in z-direction
   real     intent(in)  :: rod_width   !width at x=0 plane

   real, dimension(nx,ny,nz), intent(out) :: c !progress variable
!-----------------------------------------------------------------------
 ! local declarations
```

```
   integer i,j,k
   real width,Ly,Lx,Lz,r

   real prof(ny)
!-----------------------------------------------------------------------
 ! executable statements
!-----------------------------------------------------------------------
!-----------------------------------------------------------------------
 ! setup meeting flame fronts (1D)
!-----------------------------------------------------------------------
   elseif(i_fgeo.eq.4)then

 ! set params
      Lx=xmax-xmin

 ! fill x-y plane
      do j=1,ny
         c(:,j,1) = 1-(tanhProf(nx,nx_g,Lx, &
                        x,trans_width,1.0,x_centre) * &
               (1.0-tanhProf(nx,nx_g,Lx,x,trans_width, &
                             1.0,Lx-x_centre)))
      enddo
!-----------------------------------------------------------------------
 ! setup circular planar flame progress variable
!-----------------------------------------------------------------------
   elseif(i_fgeo.eq.5)then

 ! x_centre :: Centre of circular flame, x-dir
 ! y_centre :: Centre of circular flame, y-dir
 ! rod_width :: Distance centre of circular flame
 !              to midpoint of transition

 if(vary_in_x==1.AND.vary_in_y==1.AND.vary_in_z==0) then
 ! set params
  !    Lx=xmax - abs(xmin)
 ! fill x-y plane
      do i=1,nx
        do j=1,ny
```

```
          r=sqrt((x(i)-x_centre)**2 + (y(j)-y_centre)**2)
          c(i,j,1) = tanhProf2(r,trans_width,1.0,rod_width)
        enddo
      enddo

elseif(vary_in_x==1.AND.vary_in_y==0.AND.vary_in_z==1) then
! fill x-z plane
      do k=1,nz
        do i=1,nx
          r=sqrt((x(i)-x_centre)**2 + (z(k)-z_centre)**2)
          c(i,1,k) = tanhProf2(r,trans_width,1.0,rod_width)
        enddo
      enddo

elseif(vary_in_x==0.AND.vary_in_y==1.AND.vary_in_z==1) then
! fill y-z plane
      do k=1,nz
        do j=1,ny
          r=sqrt((y(j)-y_centre)**2 + (z(k)-z_centre)**2)
          c(1,j,k) = tanhProf2(r,trans_width,1.0,rod_width)
        enddo
      enddo

else
   write(*,*) 'No match, stop iteration'
   stop
endif
!-----------------------------------------------------------------
! setup spherical 3d flame progress variable
!-----------------------------------------------------------------
   elseif(i_fgeo.eq.6)then

! x_centre :: Centre of spherical flame, x-dir
! y_centre :: Centre of sperical flame, y-dir
! z_centre :: Centre of spherical flame, z-dir
! rod_width :: Distance from centre of spherical flame
!              to midpoint of transition

! fill x-y-z
```

```
      do k=1,nz
        do i=1,nx
          do j=1,ny
            r=sqrt((x(i)-x_centre)**2 + &
                   (y(j)-y_centre)**2 + (z(k)-z_centre)**2)
            c(i,j,k) = tanhProf2(r,trans_width,1.0,rod_width)
          enddo
        enddo
      enddo

    endif

  function tanhProf2( s, w_trans, A_trans, L_o) result(f)
  !   routine by james sutherland,
  !   modified by Andrea Gruber 2005/03/01
  !   modified by Nikolai Austarheim 2012/07/05
    !-------------------------------------------------------!
      ! Generates a profile transitioning from 0 to 1      !
      !~~~~~~~~~~~~~~~~~~~~~~~~~~~~~~~~~~~~~~~~~~~~~~~~~~~~~!
      ! s         - Spatial position of grid points(local)!
      ! w_trans   - width of transition                    !
      ! A_trans   - amplitude of transition               !
      ! L_o       - midpoint of transition                !
       !-------------------------------------------------------!
      implicit none
       real, intent(in) ::  w_trans, A_trans, L_o, s
       real, intent(out) :: f
         f = 0.5*A_trans * ( 1.0 + tanh( (s-L_o)/w_trans ) )
      return
    end function tanhProf2
!-----------------------------------------------------------------
    end subroutine set_c_prof
!=================================================================
```

E Fortran Source Code - Initialize flame

Attached is some of the source code in init_flame.f90 which initializes many of the characteristics of the flame. The code is kept at a bare minimum to keep the thesis at a reasonable length (some unrelevant cases has been excluded).

Here the code for getting the input parameters, setting several key parameters, initializing a velocity field, and calling functions to calculate the flame characteristics are included.

```
!=======================================================================
  subroutine initialize_flame( io )
!=======================================================================
! initializes premixed planar or v-flame by prescribing
! c-variation in space and using table lookup for c
! Evatt Hawkes July 2003,
! modified by Andrea Gruber 2008/04/15
!-----------------------------------------------------------------------
  use topology_m
  use variables_m
  use reference_m,
  only : t_o,t_ref,a_ref,p_ref,pres_atm,l_ref,univ_gascon
  use param_m, only : nx,ny,nz,n_spec,nx_g,ny_g,nz_g
                      vary_in_x,vary_in_y,vary_in_z
  use runtime_m, only : i_restart
  use clookup_m,
  only : clookup,calc_rho0,initialize_clookup,clookup_1val
  use chemkin_m, only : species_name
  use thermchem_m,
  only : avmolwt, calc_inv_avg_mol_wt, i_react

  use feedTurb_m,    only : meanVel, vel_bar
  use turbulence_m

  use grid_m,
  only : xmax,xmin,delx,ymax,ymin,dely,zmax,zmin,delz,x,y,z

  use flame_anchor_m,
  only :     i_internal_anchor, y_anchor, temp_anchor,  &
             i_g_anc_s,i_g_anc_e,                       &
```

```
                j_g_anc_s,j_g_anc_e,                                    &
                k_g_anc_s,k_g_anc_e,                                    &
                is,il,js,jl,ks,kl,is_anchor_proc,                       &
                initialize_internal_anchor, smt_anchor,                 &
                n_anc_hw, y_anc, t_anc, t_anc_init

  implicit none

!-----------------------------------------------------------------------
! declarations passed

  integer,                intent(in)  :: io       !io unit

!-----------------------------------------------------------------------
! local declarations

  character*100 :: filename                                     &
  !input filename
  integer :: io_vf=13                                           &
  !io unit for input file
  real, dimension(nx,ny,nz)    :: c, d                          &
  !progress variable - used for tabulation
  real, dimension(ny,nz)       :: vel_bar_xinlet &
  !mean velocity at x-inlet plane

  integer :: i_fgeo, i_ferr  !flame geometry flag
  real tan_alpha    ! tan of half angle
  real st_est       ! estimated turbulent flame speed (cm/s)
  real u_inlet      ! inlet speed (cm/s)
  real rod_width    ! width of "stabilising rod" -i.e.
                    ! width of c-profile at inlet (mm)
  real trans_width  ! thickness of c-profile
                    ! - O(delta thermal) (mm)
  real x_centre     ! x position of rod (mm)
  real y_centre     ! y position of rod (mm)
  real z_centre     ! z position of rod (mm)
  real press_in     ! inlet pressure (atm)
  real a            ! Dummy variable
```

```
  real rho0         ! inlet density at c=0
  real rhoL         ! outlet density at c=1
  real rhou_inlet   ! inlet mass flux based on u_inlet
                    ! and rho0

  real u_inlet_temp! Used for 2D case

  real fact1 !temporary


  integer L,i,j,i_x_pos,j_y_pos


!-----------------------------------------------------------------
! executable statements
!-----------------------------------------------------------------
!-----------------------------------------------------------------
! read the control file
!-----------------------------------------------------------------
  filename='../input/flame.in'
  call inquire_about_input_file(filename,io)
!-----------------------------------------------------------------
! myid==0 only opens and reads file
  if(myid.eq.0) then
!-----------------------------------------------------------------
!   open file

     open(unit=io_vf,file=trim(filename),status='old')
!-----------------------------------------------------------------
!   read header
     read(io_vf,*)
!   read flame geometry flag
     read(io_vf,*) i_fgeo
!   read flame anchor flag
     read(io_vf,*) i_internal_anchor
!   read width of "stabilising rod"
!   - ie width of progress variable
!   profile at inlet
     read(io_vf,*) rod_width
```

```
!   read mean inlet speed
     read(io_vf,*) u_inlet
!   read turbulent flame speed estimate
     read(io_vf,*) st_est
!   read rod centre point in x-direction
     read(io_vf,*) x_centre
!   read rod centre point in y-direction
     read(io_vf,*) y_centre
!   read rod centre point in z-direction
     read(io_vf,*) z_centre
!   read transition width
     read(io_vf,*) trans_width
!   read pressure
     read(io_vf,*) press_in
!   close file
     close(io_vf)
  endif

!-------------------------------------------------------------
! write header
  if(myid.eq.0) then
      elseif(i_fgeo.eq.4) then
        write(io,*) 'initializing meeting flame fronts...'
        write(io,*)
      elseif(i_fgeo.eq.5) then
        write(io,*) 'Initializing circular 2D flame...'
        write(io,*)
      elseif(i_fgeo.eq.6) then
        write(io,*) 'Initializing spherical 3D flame...'
        write(io,*)
     else
        i_ferr=1
     endif
  endif

! terminate run if wrong flag
  if(i_ferr.eq.1) then
     if(myid.eq.0) write(io,*)
     'Error in init_flame: correct i_fgeo'
```

```
      'or i_internal_anchor!'
     call terminate_run(io,0)
     !must be called by all processors
   endif

! broadcast flags
   call MPI_Bcast(i_fgeo,1,MPI_INTEGER,0,gcomm,ierr)
   call MPI_Bcast(i_internal_anchor,1,
                  MPI_INTEGER,0,gcomm,ierr)

! broadcast velocities, rod position and pressure
   call MPI_Bcast(rod_width,1,MPI_REAL8,0,gcomm,ierr)
   call MPI_Bcast(u_inlet,1,MPI_REAL8,0,gcomm,ierr)
   call MPI_Bcast(st_est,1,MPI_REAL8,0,gcomm,ierr)
   call MPI_Bcast(x_centre,1,MPI_REAL8,0,gcomm,ierr)
   call MPI_Bcast(y_centre,1,MPI_REAL8,0,gcomm,ierr)
   call MPI_Bcast(z_centre,1,MPI_REAL8,0,gcomm,ierr)
   call MPI_Bcast(trans_width,1,MPI_REAL8,0,gcomm,ierr)
   call MPI_Bcast(press_in,1,MPI_REAL8,0,gcomm,ierr)

! nondimensionalise
   u_inlet=u_inlet/(a_ref*100.0)              !from cm/s
   st_est=st_est/(a_ref*100.0)                !from cm/s
   press_in=press_in/p_ref*pres_atm           !from atm
   rod_width=rod_width/(l_ref*1000.0)         !from mm
   x_centre=x_centre/(l_ref*1000.0)           !from mm
   y_centre=y_centre/(l_ref*1000.0)           !from mm
   z_centre=z_centre/(l_ref*1000.0)           !from mm
   trans_width=trans_width/(l_ref*1000.0)     !from mm

! set tan of V-flame angle:
   tan_alpha=st_est/sqrt(u_inlet**2-st_est**2)

! set pre-anchor mean temperature
   t_anc_init=t_o/t_ref

! set the c-profile
   call set_c_prof(c,tan_alpha,trans_width,x_centre,
                   y_centre,z_centre,rod_width,i_fgeo)
```

```
! now filter the c-profile
! (when approaching the wall boundaries)
  call filter_u(nx,ny,nz,1,c)

! if not reacting, just set c=0.0
  if(i_react==0)then
    c(:,:,:)=0.0
  endif

! do c-lookup
  call clookup(c,yspecies,temp,io)

! calculate the fresh gas density
  call calc_rho0(rho0, rhoL, press_in, io)

! deallocate c-table lookup
  call initialize_clookup(io,-1)

! set mass flux based on inlet speed
  u_inlet_temp = 2500.0
  u_inlet_temp = u_inlet_temp/(a_ref*100.0)
  !rhou_inlet=u_inlet_temp*rho0

! calculate inverse of average molecular weight
  call calc_inv_avg_mol_wt(yspecies,avmolwt)

! set pressure
  pressure(:,:,:)=press_in

! set density from equation of state - use d as temporary
  fact1=univ_gascon*(1.0/a_ref**2)*t_ref
  d(:,:,:)=pressure(:,:,:)/(fact1*temp(:,:,:)*avmolwt(:,:,:))

! set local x-velocity based on conservation of momentum
! in x-direction
!  u(:,:,:,1)=rhou_inlet/d(:,:,:)

! set velocity in y and z directions
```

```
!!$  u(:,:,:,1)=u_inlet  !for constant velocity
!  u(:,:,:,2:3) = 0.0

do j=1,ny
  do i=1,nx
    a = abs(atan((y(j)-y_centre)/(x(i)-x_centre)))
    if((y(j)-y_centre).GT.0 .AND. (x(i)-x_centre).GT.0)
    then
      u(i,j,:,1) = u_inlet_temp*cos(a)*c(i,j,1)
      u(i,j,:,2) = u_inlet_temp*sin(a)*c(i,j,1)
    elseif((y(j)-y_centre).LT.0 .AND. (x(i)-x_centre).GT.0)
    then
      u(i,j,:,1) = u_inlet_temp*cos(a)*c(i,j,1)
      u(i,j,:,2) = -u_inlet_temp*sin(a)*c(i,j,1)
    elseif((y(j)-y_centre).LT.0 .AND. (x(i)-x_centre).LT.0)
    then
      u(i,j,:,1) = -u_inlet_temp*cos(a)*c(i,j,1)
      u(i,j,:,2) = -u_inlet_temp*sin(a)*c(i,j,1)
    elseif((y(j)-y_centre).GT.0 .AND. (x(i)-x_centre).LT.0)
    then
      u(i,j,:,1) = -u_inlet_temp*cos(a)*c(i,j,1)
      u(i,j,:,2) = u_inlet_temp*sin(a)*c(i,j,1)
    endif
  enddo
enddo
u(:,:,:,3) = 0.0


! now apply top-hat filter to the field
! (when approaching the wall boundaries)
  call filter_u(nx,ny,nz,3,u)

  if(xid==0) then
     vel_bar_xinlet = u(1,:,:,1)
  endif

  call MPI_Bcast(vel_bar_xinlet,ny*nz,
                 MPI_REAL8,0,xcomm,ierr)
```

```
      meanVel = u_inlet ! This set the same convective/scan
                        !velocity for all processors
      allocate(vel_bar(ny,nz))
!       vel_bar = vel_bar_xinlet
 vel_bar = u(1,:,:,1)
!!$  endif
!u(:,:,:,1:2)=c(:,:,1)*u(:,:,:,1)

!N allocate(vel_bar_x(nx,ny,nz))
!N vel_bar_x = u(:,:,:,1)

!N allocate(vel_bar_y(nx,ny,nz))
!N vel_bar_y = u(:,:,:,2)

!-----------------------------------------------------------------
  return
  end subroutine initialize_flame
=================================================================
```